UNIVERSITY OF TWENTE.

Signals & Systems

MSc Thesis

Design and analysis of a flat sound generator

Author:
Juan Carlos Villamil O.
s0091669
University of Twente
Department of Electrical Engineering,
Mathematics and Computer Science
(EEMCS)
Signals and Systems group (SAS)
j.c.villamil@student.utwente.nl

Examination Committee:
Dr. ir. A.P. Berkhoff
Prof. Dr. Ir. C.H. Slump
Ir. E.R. Kuipers
MSc. H. Ma

Report code: EWI/SAS 2012 - 015

August 23, 2012

Abstract

In this report, the design, mathematical verification and practical validation of a flat sound generator will be presented. The generator consists of a thin sheet of aluminium and a 50% perforated steel plate, connected to each other with a sandwiched aluminium honeycomb structure. With this configuration, the system benefits from high stiffness properties without compromising too much in mass. To improve the performance of the system, active control is implemented. For obtaining a flat frequency response around the resonance frequency, a feedback control algorithm is applied. A feedforward control method is used to extend the frequency response in the low frequencies. The system is characterized by means of the Thiele/Small parameters, the electrical impedance and the radiated SPL.

Contents

Chapter 1

Introduction

Conventional loudspeakers have been used and developed for decades. However, new applications where size, weight, shape or even aesthetics are an issue, require alternative designs. In a special way, placement in locations where the space available is limited, and where the use of active control techniques is attractive, like ventilation tubes or aircraft cabins ask for powerful devices with reduced dimensions. Lot of research has been done on flat loudspeakers[6, 7]. Some companies, like Sonance[3], Glas Platz[1] and Sound Advance[4], have developed flat and 'invisible' loudspeakers for the consumer market. However, most of these alternative designs perform poorly in the low frequencies (as will be seen below). In this chapter a review is given about the conventional loudspeaker and, after that, some of the alternative techniques, which have abandoned the pistonic operation, are discussed. The chapter ends with a discussion on the techniques, after which the outline of this thesis is presented.

1.1 Conventional loudspeaker techniques

In this section, a short review on existing loudspeaker technologies will be given. Those technologies include the pistonic loudspeakers, DM Loudspeakers and EAP loudspeakers, among others.

1.1.1 Pistonic loudspeakers

The most common class of loudspeaker is the so-called voice-coil loudspeaker, in which the moving part is either a conic or a planar diaphragm, driven by a voice-coil motor. A cross sectional schema of a conventional pistonic loudspeaker is found in Figure 1.1. The diaphragm aims at achieving pistonic motion, hence the also commonly used name " pistonic loudspeaker". Direct-radiator loudspeakers are loudspeakers where the output is directly coupled to the air, without any acoustical impedance devices (like horns)[38]. For low frequencies, where the wavelength is large compared to the dimension of the diaphragm, the acoustic radiation mechanical resistance is low, and, considering the diaphragm to be sufficiently stiff, it moves as a whole. As the frequency increases, the mechanical resistance increases with a rate of 12 dB per octave (see Figure 1.2)

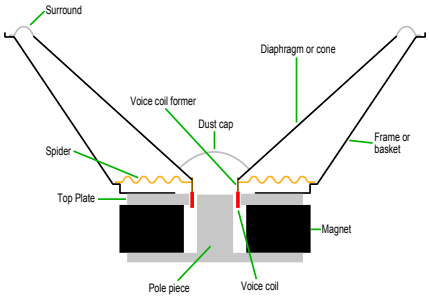

Figure 1.1: *Cross section of a pistonic loudspeaker. Source [23]*

and, if the coil is driven by a constant force, a constant acceleration (due to Newton's second law, $F = mA$, where the mass is also constant) will cause the velocity to decrease at the same rate as the (radiation) resistance increases, resulting in constant power. As long as the wavelength of the produced sound is longer than 3 times the driver diaphragm circumference, i.e. within the *piston range*[38] of the loudspeaker driver, the radiated acoustic output will be essentially nondirectional[13, p. 188]. However, when the wavelength is close to the dimensions of the diaphragm, the real part of the radiation resistance becomes constant (the inflection point in Figure 1.2) and, since the velocity continues to decrease, the total acoustic power output begins to decrease. This decrease of power does not cause a decrease in the sound level, but leads to a directional behaviour of the speaker, in which the angles become sharper with an increase in frequency[5, 31]. A straight-forward logical solution for this problem would be to use smaller diaphragms, forcing the bending point to move to a higher frequency. However, for the low frequencies where a large volume of air has to be displaced, this would imply an extensive cone displacement. This explains the fact that when an extended frequency range has to be covered, a configuration with more than one loudspeaker, combined in a so-called crossover configuration, is often used.

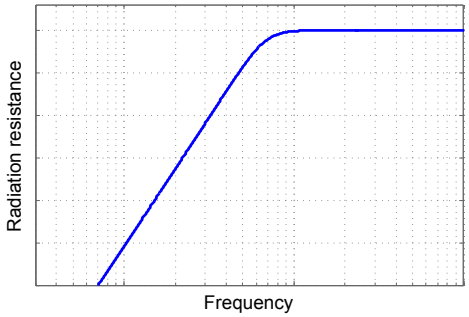

Figure 1.2: *Mechanical resistance of a pistonic loudspeaker*

On the other side, high frequencies introduce mechanic vibration modes in the diaphragm[13]. A significant part of loudspeaker design research is done to suppress this effect, by increasing the stiffness of the diaphragm (for instance, look at Olson's chapter in [31] dedicated to diaphragms and suspensions).

The pistonic behaviour of this kind of loudspeaker has another side-effect: The diaphragm emits waves in both the front and the back side, in counter phase. Extended research has also been done in minimizing the audible effect of the interference between these two wave 'sources'. The most common method used is by placing the loudspeaker in a baffle or an enclosure. There are several types of enclosures: Open-back, closed, acoustical labyrinth[31]. Bass-reflex (or acoustical phase inverter) enclosures use an open cavity which, in combination with the chamber, behaves like a Helmholtz resonator[19]. In the frequency region between the Helmholtz resonance frequency and the natural resonance frequency of the diaphragm, the phase of the velocity inside the cave is inverted in such a way that the waves in the back 'reinforce' the waves in the front, creating more output power. For a more extensive review on loudspeaker types, refer to [23].

1.1.2 Distributed Mode Loudspeakers (DML)

In contrast with pistonic loudspeakers, in which the moving part is supposed to act like a rigid body (i.e. the whole structure moves with the same acceleration to have the behaviour of a lumped moving mass), Distributed Mode Loudspeakers (DML) are characterised by a randomly moving diaphragm. The diaphragm is excited by a large number of (vibration) modes, in different amplitudes and frequencies. DM loudspeakers deliver power to the mechanical resistance of the diaphragm, which is constant with frequency, and do not encounter resistance due to the radiation itself, like conventional loudspeakers[5]. As a consequence of this fact, distributed mode loudspeakers are uniformly diffuse in all frequencies they operate. However, when low frequencies have to be reached by a DM system, a conventional loudspeaker has to be used[27, 12].

1.1.3 Electrostatic loudspeakers

Electrostatic loudspeakers (ESL) have been developed for years (the first record of an electrostatic device dates from 1917[11]). An ES loudspeaker consists of a thin diaphragm (usually a strong polymer) suspended in an electrostatic field, created by two stationary, conducting electrodes. The diaphragm is usually separated by the electrodes by a narrow gap as schematically seen in Figure 1.3. When an alternating (driving) current is added to a direct (biasing) current

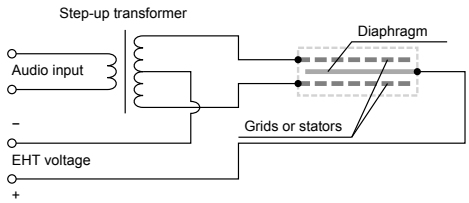

Figure 1.3: *Electrostatic loudspeaker*

and is applied to the electrodes, the diaphragm oscillates and produces sound.

Typical amplitudes are several thousands volts[36]. Electrostatic loudspeakers cover a wide frequency range, from about 1000 Hz until ultra-sound levels[24].

1.1.4 (Dielectric elastomer) Electroactive Polymers (EAP)

Electro-Active polymers, or EAPs, are polymers with the property of changing in shape and/or size when an electric stimulation is applied. Since the early 90s, materials have been studied which allow a significant size (or shape) change, fact that made this materials attractive for numerous technological applications[39, 10]. Heydt et.al. developed and demonstrated a dielectric EAP loudspeaker[36], based on this principle. Their design uses a thin polymer film, electroded on both sides which, when an electrical field is applied, changes its shape. Properly mechanical biasing allows it to oscillate in a consistent direction to produce undistorted sound[40]. The loudspeaker produces a relatively flat frequency response for frequencies above 1kHz[35].

1.1.5 ElectroMechanical Film (EMFi) loudspeakers

Also related to ES loudspeakers are the so-called Electromechanical film (EMFi) loudspeakers. "The ElectroMechanical Film - EMFi is a thin, cellular, biaxially oriented polypropylene film that can be used as an electret"[29]. An electret material has the property of remaining permanently charged when it has been subjected to a strong electrical field during its manufacturing. The working principle of an EMPi loudspeaker is similar to the electroactive polymers: When applying a voltage to the metallized film (with electrode operation), variations in the film thickness produce a sound wave[9].

All these alternative (flat) designs have one thing in common: They perform poorly in the low frequencies. In this project, a new flat loudspeaker system is presented and characterised. As will be seen in the next section, it consists of a thin aluminum plate, reinforced with an aluminum honeycomb structure and a perforated RVS plate to provide enough stiffness for pistonic operation. An enclosure of Perspex completes the system, being conventional rubber the material which confines the air inside the cavity. Four external springs will support the plate and hold it in equilibrium position.

1.2 Thesis outline

In the next chapter, the mathematical and theoretical background for modelling of the flat sound generator will be given. Characteristics of the system will be discussed, from the electric, acoustic and mechanical point of view. The chapter will end with a model of the loudspeaker and two control techniques to improve the frequency response. In Chapter 3, a computer model built in Matlab will be fully simulated to prove the validation of the theoretical concepts. A previously made structural model of the system is also briefly discussed. Chapter 4 shows some of the practical design choices that were be made while building the physical device. Some pictures and description of the building process are discussed in this chapter. Measurements, structural and elecrrical, on the finished system are presented in Chapter 5, where the sound generator is

characterized by the usual parameters. The chapter finishes with a comparison with an existing comercial driver. After that, conclusions of the project and recommendations for further research will be given in Chapter 6.

Chapter 2

Mathematical modelling and verification

The configuration of the loudspeaker subject to study in this project is described by Berkhoff in [16]. Figure 2.1 shows a schematic side view of the loudspeaker. The sound radiating surface is an aluminium plate (1), with an aluminium honeycomb structure (2) to provide enough stiffness[18]. On the back side of the honeycomb (the lower side), a perforated aluminium plate (3) is placed. Since the irregularities in the perforated plate and the honeycomb are small compared to the wavelength, they do not interfere significantly in the emitted sound power[34]. The driving mechanism is a system of voice-coil motor(s) (omitted in the figure), which move parts 1, 2 and 3 with the same displacement. The air inside the cavity is isolated from the outside world by the rubber suspension (4), creating a closed enclosure.

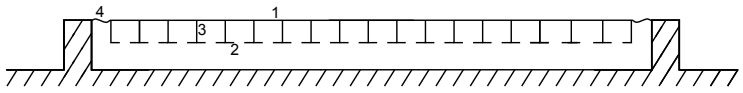

Figure 2.1: *Schematic configuration of the generator*

This chapter starts with a short review of some important acoustic quantities. After that, with the knowledge that loudspeaker performance is strongly dependent on the parameters of the loudspeaker, such as maximum electrical and acoustical power, peak cone excursion and flatness of the frequency response, the system parameters of this specific configuration will be derived and discussed, whereafter a short review on the mechanical behaviour of such systems will be given The chapter will end with a discussion on how to improve the performance of the system.

2.1 Acoustics - A short review

In this section a short review on acoustics will be given. The concepts treated are essential for the derivation of the mathematical model in the next section. In the first part, the basic principles about propagation of sound will be presented.

After that some concepts in acoustics used in this report will be briefly exposed. A more extensive derivation can be found in any book on acoustics, like [19].

2.1.1 Sound and vibration

Waves

In physics, a wave is the propagation of the perturbation of a property of a medium (like density, pressure or electromagnetic field) through that medium. A wave implies a transport of energy without transport of any material. The most important properties of a wave are the amplitude, the wavelength (spatial period) and the time period. The frequency is the inverse of the time period.

Longitudinal waves

A longitudinal wave is a wave in which the oscillation motion of the particles is parallel to the propagation direction of the wave. Longitudinal waves also known as compression waves.

Sound waves

Sound is the name given to audible waves that produce oscillation in the pressure of air (or any other fluid, solid or gas). In solids, the propagation of sound involves variations of the tensional state of the medium. The vibrations are produced in the same propagation direction of the sound, which means that the sound waves are longitudinal.

Propagation of sound

As mentioned in the last section, propagation of sound involves transport of energy without transporting matter through a medium, in the form of longitudinal waves. Certain characteristics of the medium influence the sound waves. In general, sound propagates much faster in solid and liquid materials than in gasses. The more the compressibility $(1/K)$ of the medium, the less the speed of the sound through it. Density (ρ) plays also a mayor (destructive) role in the propagation speed. Summarizing,

$$v \propto \sqrt{\frac{K}{\rho}} \tag{2.1}$$

In gasses, temperature influences both compressibility and density. This makes the temperature the crucial factor which determines the speed. In the air, sound has a velocity of 331,3 m/s when the temperature is 0°C, and the atmospheric pressure is 1 ATM (at sea level). It is related to the temperature through

$$v_s = v_0 + \beta T, \tag{2.2}$$

where

- $v_0 = 331.3$ m/s
- $\beta = 0.606$m/(s oC)

- T is the temperature in Celsius

At 20°C, the speed of sound in air is 343.2 metres per second (1236 km/h). At 15°C, the speed of sound in air is 340 m/s (1224 km/h). This value corresponds to 1 MACH.

Vibration

A vibration is defined as the propagation of elastic waves which produce tensions and deformations on a continuous medium (or equilibrium position)

Nearfield and Farfield

In acoustics, nearfield is the region close to a source where the sound radiated by the source and the particle velocity are not in phase. At a distance known as the Raileigh distance (defined as the piston area divided by the wavelength), the sound field becomes more stable and propagation is more uniform: the farfield. In principle, in the farfield, the sound radiated by a source decays at a rate of 6 dB each time the distance (from the source) is doubled.

2.1.2 Acoustical quantities

Acoustic impedance

In general terms, and impedance is described as the ratio of a push or effort variable (as it will be seen later) to a corresponding flow variable. In acoustics, the *specific* acoustic impedance is defined as the ratio of the pressure at a point to the particle velocity at the same point, as

$$Z_{ac}(s) = \frac{p(s)}{u(s)} \tag{2.3}$$

The acoustic impedance is measured in MKS rayls, where 1 rayl is equivalent to 1 pascal-second per meter (Pa s/m), and to 1 Newton-second per cubic meter ($\mathrm{Ns/m^3}$).

Sound intensity

The sound intensity I in a specified direction is, by definition, the time average of unit flow through an unit area. If $\mathbf{i} = p\mathbf{u}$ is the instantaneous energy flow per unit area, the sound intensity (a vector) is defined as

$$\mathbf{I} = \frac{1}{t_{av}} \int_0^{t_{av}} p\mathbf{u}dt \tag{2.4}$$

If I is assumed to be in the direction of propagation, the sound intensity is a scalar relation (since no power flows in a direction perpendicular to the particle velocity)

$$I = \frac{1}{t_{av}} \int_0^{t_{av}} pudt \tag{2.5}$$

Acoustic power

The acoustic power (of sound power) W passing through a defined surface S is the integral of the intensity over that surface

$$P_A = \int_S \mathbf{I} d\mathbf{S} \tag{2.6}$$

In the case of a duct where the intensity is uniform over its cross sectional area, the expression for the sound power reduces to

$$P_A = IS \tag{2.7}$$

In the case of an omnidirectional outgoing spherical wave crossing the surface S of a sphere of radius r, it becomes (since the intensity is constant over the surface)

$$P_A = 4\pi r^2 I \tag{2.8}$$

Sound Pressure Level (SPL)

The sound pressure level (SPL) is a logarithmic measure of the pressure of sound, and is defined as

$$\text{SPL} = 20 \log_{10} \left| \frac{p_{rms}}{p_{ref}} \right|, \tag{2.9}$$

where $p_{ref} = 20 \cdot 10^{-6}$ Pa, and corresponds (approximately) to the threshold of hearing of young persons. Therefore, a SPL of 0 dB is the threshold of hearing.

2.1.3 Sound radiation from panels

When a panel is excited from an external source, it starts vibrating with a set of so-called structural modes (which will be discussed in a latter section). Each mode has an unique vibration pattern and a radiation energy and efficiency, which determine the total radiation power of the mode. This sound power, added to the pistonic radiation power of the panel, determines the total acoustic power of a panel. In this work, the sound radiation as result of the vibration modes of the panel is neglected, and only the power produced by the pistonic work of the speaker will be taken into account.

2.2 Electromechanical properties

2.2.1 System characterisation

Assuming a voice-coil drive, the flat loudspeaker can be modelled with electrical symbols as shown in Figure 2.2[31, 15] (a detailed description of the modelling of mechanical circuits can be found in [13, chap. 3] and [31, chap. 4], see also [41]). The modelling parameters are in three domains. In the electric domain, where the voltage is the effort variable and the current the flow variable[1], e_g

[1]Here, the convention given by Breedveld[20] is used. The *effort* variable is constant is case of equilibrium between two storage elements, and the *flow* variable is the net supply rate of q-type, or *generalized displacement*, variables. Effort and flow form a *power conjugated* variable pair: Their product is equal to the power in a system.

is the driver voltage and R_e is the electrical resistance of the circuit (both the generator and the voice coil). The inductance of the voice coil, in series with the resistance, has been left as a wire, as it can be neglected for the low frequencies region.

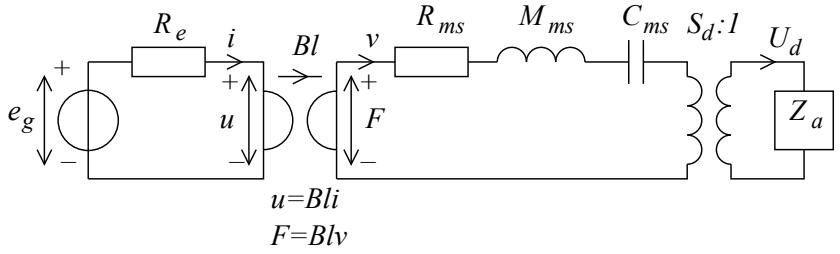

Figure 2.2: *Low frequencies equivalent circuit of a loudspeaker. Source [14]*

The voice coil couples the electrical with the mechanical circuit. Since the current through the coil is proportional to the mechamotive force (or driving force, $f_M = Bli$), it can be modelled as a gyrator with ratio Bl, where B is the flux density through the air gap and l the length of the conductor of the coil. In the mechanical domain, where the force F and the velocity v are respectively the effort and flow variables, R_{ms} represents the mechanical resistance of the suspension system and the air load, M_{ms} the combined mass of the honeycomb structure, the moving coil and the air load and C_{ms} the compliance of the suspension system. Coupling to the acoustic domain occurs by means of the area S_d of the aluminium plate, in a way that the volume velocity U_d becomes the flow variable, where the pressure p is the effort variable.

In the acoustical domain, assuming a closed enclosure, three main impedances can be identified: Z_{ab1} and Z_{ab2}, corresponding to the radiation impedance [2] of the volume of air enclosed between the perforated plate and the back plate (1) and between the two moving plates (2) respectively (defined as in Figure 2.3), and Z_{perf} the radiation impedance of the perforated sheet.

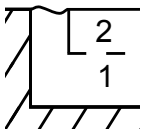

Figure 2.3: *Definition of the cavities for equivalent circuit*

According to Beranek[13, p. 117], the acoustical impedance of a volume of air has a real part, corresponding to the radiated power, and an imaginary part, accounting for the reactive power. In this case, since the frictional losses in adjacent air layers in the transmission of sound through the air are small[31], the real part (or acoustical resistance, due to viscosity of the air) can be neglected,

[2]The radiation impedance as a "quantitative statement of of the manner in which the medium reacts against the motion of a vibrating surface"[13]

which means that the impedances Z_{ab1} and Z_{ab2} can be defined as

$$Z_{ab1,ab2} = \frac{1}{sC_{ab1,ab2}} \tag{2.10}$$

for

$$C_{ab1,ab2} = \frac{V_{b1,b2}}{\rho c^2} \tag{2.11}$$

being $V_{b1,b2}$ the volume of air in the cavities 1 and 2, respectively. $\rho = 1.21$ kg/m^3 is the density of air and $c = 343$ m/s is the speed of sound in vacuum. Since the volume velocity U_1 flowing into cavity 1 equals the effective volume velocity through the perforated plate plus the volume velocity U_2 flowing into cavity 2, the total acoustic load Z_a can be modelled as shown in Figure 2.4.

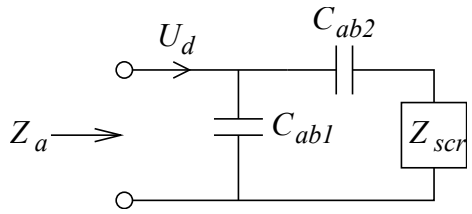

Figure 2.4: *Equivalent circuit for the acoustical impedance. Source [14]*

Using the expressions shown in Equations 2.10, Z_a is defined as

$$Z_a = \frac{1}{\frac{1}{Z_{ab1}} + \frac{1}{Z_{perf}+Z_{ab2}}} \tag{2.12}$$

Beranek[13, p. 138] introduced the acoustic impedance (ratio between pressure and velocity) of a perforated plate as a mass-resistance element, given by

$$Z_{perf} = R_{perf} + i\omega M_{perf}, \tag{2.13}$$

where

$$R_{perf} = \frac{1}{\pi a^2}\rho\sqrt{2\omega\mu}\left[\frac{t}{a} + 2\left(1 - \frac{A_h}{A_b}\right)\right] \tag{2.14}$$

$$M_{perf} = \frac{\rho}{\pi a^2}\left[t_p + 1.7a\left(1 - \frac{a}{b}\right)\right], \tag{2.15}$$

where a is the radius, $A_h = \pi a^2$ the area of the holes, and $A_b = b^2$ is the area of a square around each hole, according to Figure 2.5. The resistive part of the impedance corresponds to viscous effects of airsolid interaction, and the imaginary part, the acoustic reactance, is inertial in nature[34]. The thickness of the plate is represented by t_p. If a square plate with area S_d is assumed and the porosity of the plate σ (perforation ratio in [33]) is defined as the ratio of the total area of the holes to the total area of the plate, including the holes, Equations 2.14 and 2.15 can be rewritten as (in the case of a square radiating

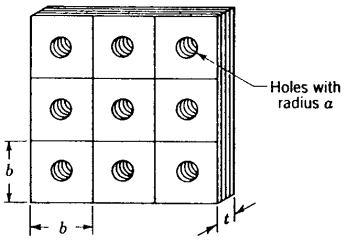

Figure 2.5: *Perforated plate of thickness t with hole radius a. Source [13]*

area)

$$R_{perf} = \frac{2\rho c}{S_d \sigma}\sqrt{\frac{2\mu k}{c}}\left(\frac{t_p}{d_h} + 1 - \frac{\pi}{4}\frac{d_h^2}{g_g^2}\right) \tag{2.16}$$

$$M_{perf} = \frac{\rho}{S_d}\left(t_p + 0.85 d_h\left(1 - \frac{d_h}{2g_g}\right)\right), \tag{2.17}$$

as function of the hole diameter $d_h = 2a$ and the distance between the holes $g_g = b$, related to the porosity by

$$\sigma = \frac{\pi}{4}\frac{d_h^2}{g_g^2} \tag{2.18}$$

The wave number is given by $k = \frac{\omega}{c}$ and the dynamic viscosity by $\mu = 1.846 \cdot 10^{-5}$ N $\cdot$ s/m^2. Equation 2.13 can then be written as

$$Z_{perf} = \frac{\rho c}{S_d}\zeta_{perf}, \tag{2.19}$$

where the normalized acoustic impedance ζ_{perf} is given by

$$\zeta_{perf} = \frac{2}{\sigma}\sqrt{\frac{2\mu k}{c}}\left(\frac{t_p}{d_h} + 1 - \frac{\pi}{4}\frac{d_h^2}{g_g^2}\right) + i\left(k\left(t_p + 0.85 d_h\left(1 - \frac{d_h}{2g_g}\right)\right)\right), \tag{2.20}$$

Equation 2.20 is valid in the frequency range in which the hole diameter d_h satisfies the inequality

$$\frac{0.02}{\sqrt{f}} \leq d_h \leq \frac{20}{f} \tag{2.21}$$

Inspired by Maa [26], Putra introduces expressions for the real and imaginary parts of Equation 2.13 as

$$R_{perf} = \frac{32\mu t_p}{d_h^2}\left[\left(1 + \frac{X_0^2}{32}\right)^{1/2}\frac{\sqrt{2}}{32}X_0\frac{d_h}{t_p}\right] \tag{2.22}$$

$$M_{perf} = \rho t_p\left[1 + \left(9 + \frac{X_0^2}{2}\right)^{-1/2} + \left(\frac{8}{3\pi}\right)\frac{d_h}{t_p}\right], \tag{2.23}$$

where X_0, defined as

$$X_0 = \frac{d_0}{2}\sqrt{\frac{\omega\rho}{\mu}} \tag{2.24}$$

is the perforation constant, which includes the friction effect between the air and the plate interface in the hole, due to viscous effects. This expressions are valid when the distance between the holes is short enough compared with the acoustic wavelength[33]. This expression still has to be studied, and the implications for $\sigma \approx 50\%$.

2.2.2 Thiele/Small parameters

According to Thiele and Small[38], the fundamental physical driver parameters are R_e, Bl, S_d, C_{ms}, M_{ms} and R_{ms}, as defined in Figure 2.2. These parameters are essential because each can be set independently and has effect on the system (small-signal) performance. However, some of these parameters are neither easy nor convenient to be measured on finished systems, and the four so-called Thiele/Small parameters are more advantageous to describe the driver with. These are the following:

- Fundamental resonance frequency of the driver f_s
- Equivalent compliance volume of the driver V_{as}
- Electromagnetic quality factor Q_{es}
- Mechanical quality factor Q_{ms}

with values

$$f_s = \frac{1}{2\pi\sqrt{M_{ms}C_{ms}}} \tag{2.25}$$

$$V_{as} = \rho_0 c^2 C_{as} \tag{2.26}$$

$$Q_{es} = \frac{T_s R_e}{C_{ms} Bl^2} \tag{2.27}$$

$$Q_{ms} = \frac{T_s}{R_{ms} C_{ms}} \tag{2.28}$$

$$\tag{2.29}$$

Besides that, the total quality factor is defined as

$$Q_{ts} = \frac{Q_{ms} Q_{es}}{Q_{ms} + Q_{es}} \tag{2.30}$$

and the time constant T_s related to the resonance frequency of the driver

$$T_s = \frac{1}{2\pi f_s} = \sqrt{M_{ms} C_{ms}} \tag{2.31}$$

The quantity C_{as} will be related to the parameters of Figure 2.2 in the next section. Qualitatively, the compliance volume of the driver (measured in litres) represents the volume of air displaced by the cone at its maximum excursion. The unitless electromagnetic quality factor describes the electrical damping of the system, as result of the induced current on the wire coil through the magnetic field, which opposes to the movement of the coil. The mechanical quality factor is a measurement for the mechanical damping of the driver.

2.2.3 System analysis

Berkhoff[15] pointed out that the electrical impedance of a loudspeaker (system) can be directly related to the acoustic equivalent circuit of the system. If all the electrical and mechanical elements of Figure 2.2 are transformed to the acoustic domain, the circuit of Figure 2.6 is obtained. The expressions of the elements are given by

$$R_{at} = \frac{Bl^2}{S_d^2 R_e} + \frac{R_{ms}}{S_d^2} \tag{2.32}$$

$$M_{as} = \frac{M_{ms}}{S_d^2} \tag{2.33}$$

$$C_{as} = C_{ms} S_d^2 \tag{2.34}$$

$$p_g = \frac{Bl}{S_d R_e} e_g(s) \tag{2.35}$$

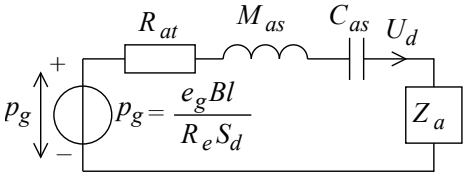

Figure 2.6: *Acoustic equivalent circuit. Source [14]*

The volume velocity $U(s)$ of de radiating plate is then given by (U is the flow variable in the acoustical domain)

$$U(s) = \frac{Z_a}{Z_a + R_{at} + sM_{as} + \frac{1}{sC_{as}}} p_g(s), \tag{2.36}$$

or, written as function of the input electrical current i_g and the (input) electrical impedance Z_{vc}

$$U(s) = i_g(s) Z_{vc}(s) X(s) \frac{sC_{as} Bl}{R_e S_d}, \tag{2.37}$$

where Z_{vc} is defined as

$$Z_{vc}(s) = \frac{e_g(s)}{i_g(s)} = R_e \frac{D(s)}{N(s)} \tag{2.38}$$

and

$$X(s) = \frac{1}{D(s)} \tag{2.39}$$

is the cone excursion. The characteristic polynomial $D(s)$ and its analogue $N(s)$ are given by, as function of the parameters given in Section 2.2.2

$$D(s) = s^2 T_s^2 + s(T_s/Q_{ts} + C_{as} Z_a) + 1 \tag{2.40}$$

$$N(s) = s^2 T_s^2 + s(T_s/Q_{ms} + C_{as} Z_a) + 1 \tag{2.41}$$

The volume velocity $U(s)$ is related to the plate velocity $v(s)$ (which is usually more convenient to measure) by the plate area

$$v(s) = \frac{U(s)}{S_d} \tag{2.42}$$

The system of Figure 2.6 has a fourth order frequency response (where the electric current is taken as input and the acoustical velocity as output). However, for the low frequencies, the compliance of the suspension C_{as} and the acoustic mass of the perforated sheet M_{perf} can be neglected, yielding the second order system whose frequency response is given by Small [38] as

$$G(s) = \frac{s^2 T_s^2}{s^2 T_s^2 + s T_s / Q_{ts} + 1}, \tag{2.43}$$

where $T_s = \frac{1}{2\pi f_s}$, and f_s is the fundamental (acoustical) resonance frequency, in this case given by

$$f_s = \frac{1}{2\pi\sqrt{M_{as} C_{ab}}}, \tag{2.44}$$

where

$$C_{ab} = \frac{C_{ab1} C_{ab2}}{C_{ab1} + C_{ab2}} \tag{2.45}$$

2.2.4 Radiated sound pressure from plate

Starting from the Rayleigh integral and using the reciprocity theorem, Berkhoff [17] derived an expression for the pressure ($\hat{p}$ in the Laplace-domain) at point x in the space within a given domain $\mathcal{D}$, due to a volume injection point source $\hat{q}$ at coordinate $\mathbf{x}^R$, when there are no volume sources in the system, as:

$$\hat{p}(\mathbf{x}^R) = \int_{\mathbf{x}\in\mathcal{D}} \hat{G}^q \hat{q} \mathrm{d}\mathbf{V} \tag{2.46}$$

where $\hat{G}$ is the Green function which gives the response due to a point source for some given acoustic boundary conditions. If the source region is taken to be symmetric in the in plane (x_3) coordinate (as shown in Figure 2.7), and its thickness Δx_3 is assumed to be infinitely small, the infinitesimal volume $\mathrm{d}\mathbf{V}$ equals the product of this thickness and the infinitesimal area of the source region $\mathrm{d}\mathbf{A}$, giving

$$\hat{q}\mathrm{d}\mathbf{V} = \hat{q}\Delta x_3 \mathrm{d}\mathbf{A} = \hat{q}'\mathrm{d}\mathbf{A}, \tag{2.47}$$

when $\Delta x_3 \to 0$. In Equation 2.47, the quantity $\hat{q}'$ is introduced, which represents the surface density of volume injection. The volume integral of Equation 2.46 turns into a surface integral in $\mathcal{S}$, the surface through the center (Figure 2.7, giving

$$\hat{p}(\mathbf{x}^R) = \int_{\mathbf{x}\in\mathcal{S}} \hat{G}^q \hat{q}' \mathrm{d}\mathbf{A} \tag{2.48}$$

For a sufficiently thin source region, the *volume* source density through the source region boundary $\partial\mathcal{D}$ can be replaced by the *surface* source density

$$\int_{\mathbf{x}\in\mathcal{S}} \hat{q}'\mathrm{d}\mathbf{A} = \int_{\mathbf{x}\in\partial\mathcal{D}} v_k \nu_k \mathrm{d}\mathbf{A} \tag{2.49}$$

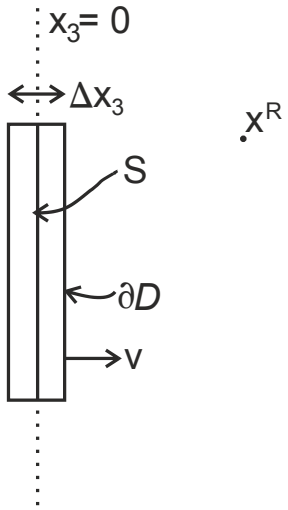

Figure 2.7: *Definitions for pressure region*

where ν is the normal unity vector to the surface. Since the area $\partial\mathcal{D}$ contains the two sides of the source, and due to the fact that for a region with vanishing thickness the source and the corresponding image source (due to the infinite baffle) coincide in space leading to an effective source with double strength when evaluating the integral in in $\mathcal{S}$, Equation 2.48 can be rewritten as

$$\hat{p}(\mathbf{x}^R) = \int_{\mathbf{x}\in\mathcal{S}} \hat{G}^q \hat{v} \mathrm{d}\mathbf{A}, \tag{2.50}$$

where

$$\hat{G}^q(\mathbf{x}^R, \mathbf{x}, s) = s\rho \frac{\exp\left(-s\frac{r}{c}\right)}{4\pi r} \tag{2.51}$$

for $r = \|\mathbf{x}^R - \mathbf{x}\|$. By definition, the value in dB is found using equation 2.9.

$$\mathrm{SPL} = 20\log_{10}\left|\frac{p}{p_{ref}}\right|, \tag{2.52}$$

2.2.5 Nearfield measurements

One of the standard parameters for a loudspeaker is the SPL radiated at half space at one meter distance. However, due to the lack of a proper anechoic room and the noisy conditions of the lab, no reliable measurements can be done, especially for the low frequencies region. Keele[21] showed that for low frequencies ($kS_d < 1$), the nearfield half space sound pressure of a loudspeaker is directly proportional to its farfield pressure. This relationship is independent on frequency and depends only on the ratio of the piston surface to the farfield distance, and is given by

$$p_n = \frac{2\pi r}{S_d} p_f \tag{2.53}$$

where r is the distance from the measuring point to the center of the loudspeaker. For the acoustic power, it holds

$$P_A = \frac{S_d}{4\rho c} p_n^2 \tag{2.54}$$

These relationships will be used when measuring pressure and power.

2.3 Structural dynamics - A short review

As mentioned in the first section of this chapter, an externally excited structure will vibrate mechanically with certain patterns called modes. Measurement of these normal (or natural) modes is an important step to be able to make the right choices about placement of the actuator, and the properties of the suspension can be derived. In this section, a short review on the structural dynamics of the sandwich structure will be given, followed by a discussion on the experimental application for measurements. Special attention will be given to the natural frequencies, mode shapes and damping conditions.

2.3.1 Frequency Response Function and Modal analysis

In this section, a Frequency-Response-Function (FRF) based approach to dynamics will be addressed. For such a system, only harmonic excitation (and thus responses) are considered. The in general complex FRF of a system, $H(\omega)$, is defined as the ratio between its harmonic response, $Xe^{j\omega t}$ to an harmonic excitation $Fe^{j\omega t}$:

$$H(\omega) = \frac{X}{F} \tag{2.55}$$

Two formulations for damping are also distinguished: viscous damping, which is proportional to the velocity, and *hysteresis* or *structural* damping, proportional to the displacement and in phase with the velocity (often called "complex stiffness").

For an undamped Single Degree Of Freedom (SDOF) mass-spring system, schematically represented in Figure 2.8 (where m is the mass and k the spring constant), the equation of motion is given by

$$m\ddot{x}(t) + kx(t) = F(t) \tag{2.56}$$

In the frequency domain, for $x(t) = Xe^{j\omega t}$, Equation 2.56 can be written as

Figure 2.8: *SDOF Mass-spring system*

$$-\omega^2 X + \omega_0^2 X = \omega_0^2 \frac{F}{k}, \tag{2.57}$$

where $\omega_0 = \sqrt{\frac{k}{m}}$ is the eigenfrequency of the undamped system. The FRF is then given by

$$H(\omega) = \frac{1}{k} \frac{1}{1 - \left(\frac{\omega}{\omega_0}\right)^2} \tag{2.58}$$

For a system with viscous damping, schematically represented in Figure 2.9 where c is the damping coefficient, the equation of motion becomes

$$m\ddot{x}(t) + c\dot{x} + kx(t) = F(t) \tag{2.59}$$

In this case, the FRF is

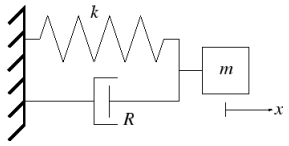

Figure 2.9: *SDOF Mass-spring-damper system*

$$H(\omega) = \frac{1}{k} \frac{1}{1 - \left(\frac{\omega}{\omega_0}\right)^2 + j2\zeta\left(\frac{\omega}{\omega_0}\right)}, \tag{2.60}$$

where the relative damping coefficient ζ is defined as

$$\zeta = \frac{c}{2m\omega_0} \tag{2.61}$$

When $0 \leq \zeta < 1$, the system is underdamped. For $\zeta = 1$, it is critically damped and for $\zeta > 1$, the system is said to be overdamped.

In the case of a harmonically excited structurally damped SDOF system (structural damping is only defined for harmonic excitation), the equation of motion is given by

$$m\ddot{x}(t) + \frac{d}{\omega}\dot{x} + kx(t) = F(t) \tag{2.62}$$

The FRF is then

$$H(\omega) = \frac{1}{k} \frac{1}{1 - \left(\frac{\omega}{\omega_0}\right)^2 + j\gamma}, \tag{2.63}$$

where the quantity $k(1 + j\gamma)$ is called the *complex stiffness*, for $\gamma = \frac{d}{k} = \frac{d}{m\omega_0^2}$.

It is worth mentioning that Equations 2.60 and 2.63 show a very similar form. This means that for slightly damped, harmonic vibrating systems at frequency $\omega \approx \omega_0$, the approximation $\gamma \approx 2\zeta$ holds.

The derivations in this section can be easily extended to Multiple Degree of Freedom (MDOF) system. As shown in the practice, most structures vibrate in multiple degrees of freedom, with complex vibration modes. This yields a phase difference between the different points of the structure, which results in a periodical back and forth movement of the modal lines. If for instance, the response of point j to a (harmonic) excitation in point i is defined as $H_{ij}(\omega)$ (in a linear case equivalent to $H_{ji}(\omega)$, the total transfer matrix will be defined as

$$H(\omega) = \begin{bmatrix} H_{11}(\omega) & H_{12}(\omega) & \cdots & H_{1n}(\omega) \\ H_{21}(\omega) & H_{22}(\omega) & \cdots & H_{2n}(\omega) \\ \vdots & \vdots & \ddots & \vdots \\ H_{m1}(\omega) & H_{m2}(\omega) & \cdots & H_{mn}(\omega) \end{bmatrix} \tag{2.64}$$

However, FRF of MDOF-systems (Equation 2.64) have seldom closed-form solutions (especially for continuous or distributed parameter systems), and in most case, practical analysis is done by means of approximate solutions. Multiple techniques and (finite element) methods have been developed to find those approximations. Discussion on those techniques will be left out in this report. More information can be found in [28] and [42].

For graphically representing the FRF's, various methods are available:

- Modulus and phase vs frequency (Bode-diagram):
- Real part and Imaginary part vr. frequency
- Real part vs imaginary part (Nyquist-diagram):

Each way has the advantages for finding the natural frequency, mode shapes and damping values.

2.3.2 Experimental measurements

In the previous section, expressions for the frequency response function for vibrating structures are discussed. In this section, some techniques for practically measuring FRF's are presented. The first step is to chose an excitation, which can be deterministic and stochastic. When making a choice, it is important to know the convolution theorem, which states that a convolution in the time domain is equivalent to a multiplication in the frequency domain. This means that a lot of work will be saved if the signals are easily transformed to the frequency domain. A special excitation signal is the impulse function, because its Fourier transform is the equivalent of the FRF. In the practise, some common excitation methods are:

- Wide-band, random or pseudo-random excitation: Contains a lot of frequencies. An excitation is called pseudo-random when the bandwidth is limited.
- Frequency sweep (also known as chirp): Contains one period per each frequency in the desired band.
- Impact method: An instrumented hammer is used as excitation. This method is rapid and easy to use, and delivers an approximately flat spectrum up to 1 kHz. For higher frequencies, it is not easy to deliver energy to a structure with an impact hammer.

As known from probability theory, the cross correlation function of two stationary, ergodic processes $x(t)$ and $y(t)$ is defined as

$$R_{xy}(\tau) = \lim_{T\to\infty} \frac{1}{2T} \int_{-T}^{T} x(t)x(t+\tau)\mathrm{d}t \tag{2.65}$$

In the frequency domain, the Fourier transform of the correlation functions is the cross spectrum S_{xy}, defined as

$$S_{XY}(\omega) = \int_{-\infty}^{\infty} R_{xy}(\tau)e^{-j\omega\tau}\mathrm{d}\tau \tag{2.66}$$

For $x(t) = y(t)$, the autocorrelation function R_{xx} and the energy spectrum S_{xx} are obtained. The relationships between these spectra and the FRF are given by

$$S_{XX}(\omega) = |H(\omega)|^2 S_{FF}(\omega) \tag{2.67}$$
$$S_{FX}(\omega) = H(\omega) S_{FF}(\omega) \tag{2.68}$$
$$S_{XX}(\omega) = H(\omega) S_{XF}(\omega) \tag{2.69}$$

For a system with input $n(t)$ and output $m(t)$ disturbances, as shown in Figure 2.10 the following relationships hold (in the frequency domain)

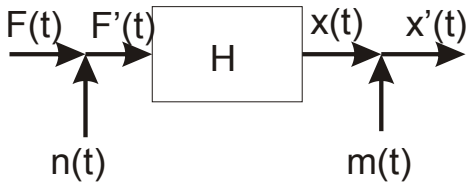

Figure 2.10: *Disturbances in the system*

$$S_{F'F'} = S_{FF} + S_{nn} + 2\mathrm{Re}[S_{Fn}] \tag{2.70}$$
$$S_{X'X'} = S_{XX} + S_{mm} + 2\mathrm{Re}[S_{Xm}] \tag{2.71}$$
$$S_{F'X'} = S_{FX} + S_{Fm} + S_{mX} + S_{nm} \tag{2.72}$$

It can be shown that when the input $F(t)$ and output $x(t)$ signals are uncorrelated with the disturbances, and the disturbances are mutually uncorrelated, the cross-terms S_{Fn}, S_{Fm}, S_{Xn}, S_{Xm} and S_{nm} are equal to zero, and the disturbances do not influence the cross spectrum. This fact explains the fact that the energy spectra and the cross spectra are frequently used to determine the FRF. Furthermore, it has the advantage that both modulus and phase information is obtained (complex quantities). The auto and cross spectra are also easily calculated from the Fourier transform of the signals.

Another important function when analysing two stochastic signals is the coherence function γ^2, defined as

$$\gamma^2 = \frac{S_{FX} S_{XF}}{S_{XX} S_{FF}}, \tag{2.73}$$

which can also written as

$$\gamma^2 = \frac{1 - \frac{S_{nn}}{S_{FF}}}{1 + \frac{S_{mm}}{S_{XX}}} \tag{2.74}$$

Equation 2.74 shows two important properties of the coherence function:

- $\gamma^2 = 1$ if there are no disturbances
- $\gamma^2 < 1$ if there are disturbances in the system

This makes the coherence function an excellent way of measuring the *quality* of a measurement.

2.3.3 Honeycomb sandwich structure

Modelling of all cells of a honeycomb structure is computationally heavy, even without taking other properties (like used glue, and structural dynamics of bended material) into account. This means that the honeycomb is usually treated as an homogeneous material with homogeneous properties. For this study, only the weight and stiffness are of importance. The fact that the wavelength of the important frequency region is much large than the irregularities of the honeycomb makes it "invisible" for the sound radiation of the plate. More detailed derivation on honeycomb (sandwich structures) can be found in [47, 37, 46, 8].

2.4 Correction for improving frequency response

From the time loudspeakers began to be used, diverse ways of obtaining a better (flatter, broader) response have been studied. In this section, two control configurations for improving the frequency response of the flat loudspeaker are proposed.

2.4.1 Velocity feedback control for additional damping

In loudspeaker systems, "the most common criterion for optimum response ... is flatness of the amplitude response over a maximum bandwidth"[38]. Since the dimension constraints of the plate and the air gap do not allow placement of powerful driving motors, the resonance of the plate will produce a high peak in the frequency response function of the system. If a velocity sensor is placed on top of the plate, and the measured velocity multiplied by a gain factor K is subtracted from the force exerted on the piston (which is proportional to the current through the coil), the excess gain can be thrown away, increasing the apparent damping of the system. This technique is referred to as active damping[32]. Furthermore, if the value of K is chosen carefully, the system will be critically damped, the resonance behaviour will not be appreciated and the control loop can be shown to be unconditionally stable: the system will tend to drive the actuator with constant velocity, and the response will fall off below the "point of ultimate resistance"[31, chap. 6]. The configuration of such a feedback control system is shown in Figure 2.11.

In case of multiple collocated actuator-sensor pairs (which means that they are

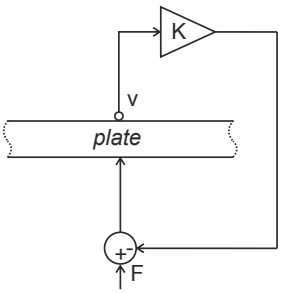

Figure 2.11: *Configuration for feedback control*

physically in the same place and energetically conjugated), where the actuator are control forces u and the sensors give velocity measurements $\dot{y}$, the governing equations of motion of a structure are

$$M\ddot{x} + Kx = f + Bu \tag{2.75}$$

$$\dot{y} = B^T \dot{x} \tag{2.76}$$

$$u = -G\dot{y} \tag{2.77}$$

where the structural damping has been neglected for simplicity. The equation includes a perturbation f and the control force u acting through the influence matrix B. G is the gain matrix (changed from K in this derivation to differentiate it from the spring constant matrix K). If G is positive definite, $u_T\dot{y} \leq 0$ and the power is dissipated, yielding a stable system. Substitution yields

$$M\ddot{x} + BGB^T\dot{x} + Kx = f \tag{2.78}$$

Equation 2.78 shows that the control forces appear as viscous damping (electrodynamic damping), where the matrix BGB^T is positive semi definite, since the actuators and sensors are collocated. Feedback control can be implemented as centralized, where one single processing unit controls all the actuators, or decentralized, where each actuator-sensor pair acts as an independent *SISO* loop, like the one shown in Figure 2.11, can be applied. It is shown by Elliott that a decentralised control system has, if tuned properly, the same performance as centralised system[22].

2.4.2 Feedforward control for extended low-frequency behaviour

In general terms, a loudspeaker shows high-pass filter behaviour, which means that, in the low-frequencies, its design can be considered as the design of a high-pass filter. However, due to the configuration of the system, the control over the configuration of the circuit is limited[41].

Ståhl [41] proposed a way to lower the cut-off frequency of the filter whose behaviour is governed by Equation 2.43. In his work, he described few ways of "taming" the mechanical components by electrical means, with different active and passive schemas, to increase the apparent moving mass and damping and to decrease the compliance. This approach was used by Normandin [30] to design networks to extend the low-frequency performance of specific loudspeaker systems with passive electric components, work extended by von Recklinghausen [44] for higher order filters. However, the complexity of the additional components influences the impedance of the whole system. As von Recklinghausen points, "Connecting a filter to the input of the amplifier, with the loudspeaker system connected to the output of the amplifier, results in a system response equal to the product of the filter response and the loudspeaker system response"[44]. These designs have an upper-frequency bound due to the voice-coil impedance[41].

A different approach can be obtained when the whole signal is prefiltered. According to Small [38], the general response of a high-pass second order filter is given by (compare to Equation 2.43)

$$G(s) = \frac{s^2 T_0^2}{s^2 T_0^2 + a_1 s T_0 + 1}, \tag{2.79}$$

where T_0 is the "nominal filter constant", and a_1 the damping coefficient. The frequency response of the loudspeaker in Equation 2.43 can be modified to the desired response function

$$G'(s) = \frac{s^2 T_{s'}^2}{s^2 T_{s'}^2 + s T_{s'}/Q_{ts'} + 1}, \tag{2.80}$$

by means of a so-called "Linkwitz" control filter with transfer function

$$L(s) = \frac{s^2 T_s^2 T_{s'}^2 + s T_s T_{s'}^2/Q_{ts} + T_{s'}^2}{s^2 T_s^2 T_{s'}^2 + s T_s^2 T_{s'}/Q_{ts'} + T_s^2}, \tag{2.81}$$

An advantage of a controller as described in Equation 2.81 is that it can be realized in real time. This fact converts it to an excellent choice for a loudspeaker controller.

Chapter 3

Computational verification

In this section, the analysis performed in sections 2.2 and 2.3 will be tested by means of extensive simulations. For the first part, from the electroacoustical point of view, simulations about the loudspeaker behaviour will be performed in MATLAB. For the structural dynamics part, a model in COMSOL will be discussed.

3.1 Electromechanical simulation

To simulate the acoustical response to an electrical excitation, the loudspeaker system is modelled in MATLAB, using the expressions found in section 2.2.3, and the expression for the acoustical impedance of Equation 2.19. The values of the parameters of the voice-coil are extracted from the data sheet (which can be found in Appendix A). The dimensions of the loudspeaker and the enclosure were modified to the real values after having built it. The value for the mechanical compliance (in Newton/meter) is extracted from measurements, as well as the value for the mechanical resistance, in Newton/m/s. The parameters are defined as shown in Listing 3.1. After that, the value of the SPL at 1 m

```
1  Nactuator = 5; % number of actuators
2  lx = 0.605;
3  ly = 0.415;
4  Sd = lx*ly; % radiator surface area
5  Vb1 = 8.e-3*Sd; % cavity volume between screen and fixed boundary
6  Vb2 = 22.e-3*Sd; % volume inside hollow plate, between screen ...
       and closed radiating surface
7  Cms = 7.78e-5;  % mechanical suspension compliance (m/Newton)
8  Mms = 1.112 + 0.010; % including air mass load (Vol_air = 0.03 x ...
       0.435 x 0.635)
9  Rms = 43.7; % mechanical suspension resistance (Newton/m/s) ...
       (beranek)
10 BL = 7.78;  % electromechanical conversion factor, from ...
       datasheet, force sensitivity (N/Amp)
11 Re = 2.6 / Nactuator; % electrical coil resistances in parallel
```

Listing 3.1: *Parameter values*

distance is found using Equations 2.50 and 2.9. Figure 3.1 shows the simulation results of the electrical impedance of the loudspeaker. It has a constant real part, except near the resonance frequency, where it behaves like an induction (under the resonance frequency) and a capacitor (above resonance frequency).

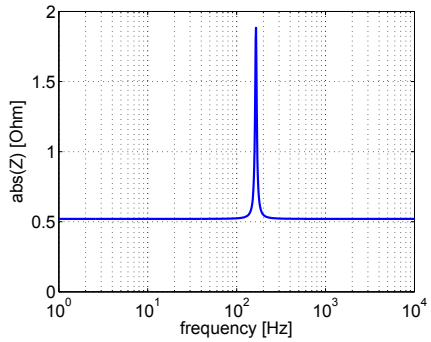

Figure 3.1: *Electrical impedance*

Figure 3.2 shows the simulation of the drive power of the loudspeaker. When no correction is applied, the power is constant. However, feedback control introduces a power drop in the resonance frequency (where power dissipation is reduced due to the fact that the excess power is "throwh away"). The power needed for amplification of the signal in the low frequencies by means of a feedforward filter can also be clearly seen.

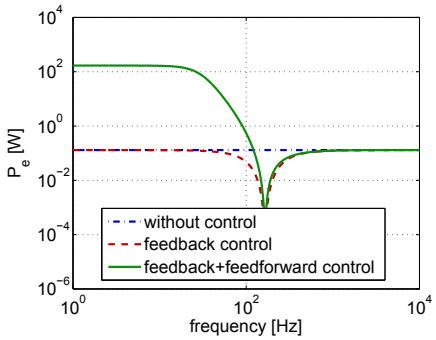

Figure 3.2: *Electrical drive power*

Figure 3.3 shows the simulated SPL radiated at 1 m distance assuming an infinite baffle. It shows a high resonance peak, flattened with the feedback control. The response is extended in the low frequencies when a feedforward filter is applied.

Figure 3.4 shows a simulation of the Nyquist plot of feedback control loop. It shows that the system is stable (even for really high gain values).

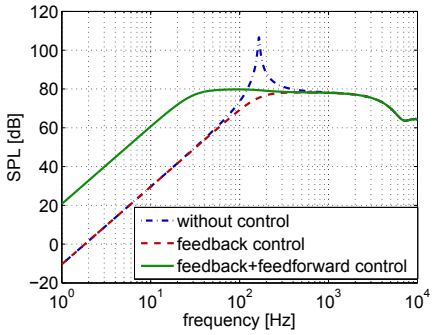

Figure 3.3: *SPL (halfspace at 1 m. distance)*

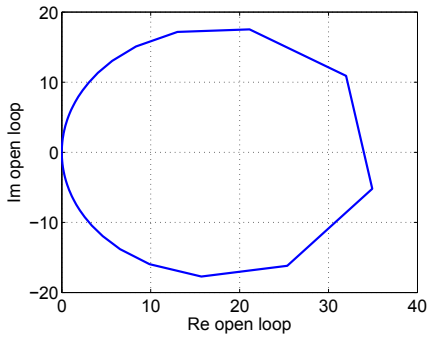

Figure 3.4: *Nyquist plot*

3.2 Structural simulation

A model of the structure was built by van Ophem in [43] in the simulation package COMSOL. COMSOL is a Finite Element Method (FEM) analysis package whose most attractive feature is the application to coupled phenomena in different domains, electrical, mechanical and acoustical, in this project. In COMSOL, a structure is divided into finite elements, which are interconnected according to a defined mesh. In this work, the radiating plate is modelled as an orthotropic material. However, the model does not perform well when simulating the vibration modes. In this work, a new model is built. As solid (radiating) plate, the aluminium sheet is taken, with 0.5 mm width. Results of the eigenfrequency analysis are shown in Figure 3.5.

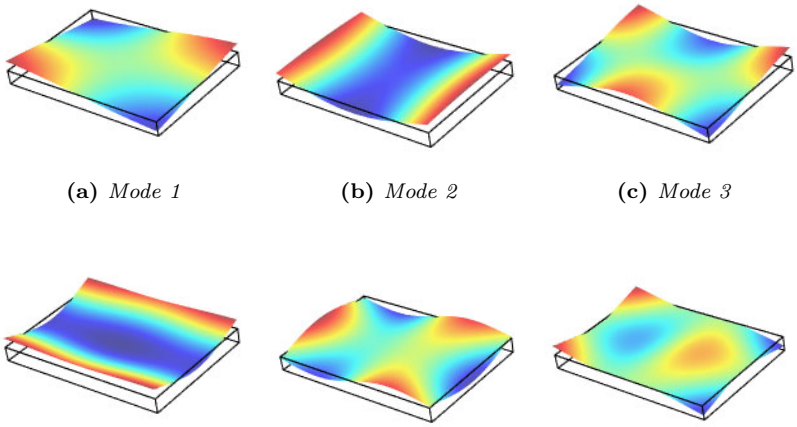

(a) *Mode 1* **(b)** *Mode 2* **(c)** *Mode 3*

(d) *Mode 4* **(e)** *Mode 5* **(f)** *Mode 6*

Figure 3.5: *Coupled modes of uncoupled plate, simulation*

However, the frequencies corresponding to the modes displayed in Figure 3.5 do not make sense. The resuts of the simulation are leave in this report for comparing the shape of the modes (and their orde).

Chapter 4

Design choices

In this chapter, some practical design choices will be presented. After that, the building of the device will be discussed from a practical point of view.

4.1 Size

As discussed in the previous chapter, the frequency response of an actuator in the low frequencies is proportional to its area. This means that for the system in this project, if a good frequency response in the low frequencies is desired, the radiator plate has to be as large as possible. However, the fabrication process of the perforated plate limits its size: The laser cutting machine at the University of Twente can only handle small plates. For the first prototype, to demonstrate the principle of work, the size was set to A4. For a more extended study (this report), a bigger generator is build, with A2 as size, as trade-off between size and cost. For fabrication of the perforated sheet, it will be manipulated as four A4 pages set together as shown in Figure 4.1. In this figure, 5 driving actuators are shown in a random configuration.

4.2 Driver

In their work, Brennan (and García Bonito)[25] discussed the need or and the requirements for actuators for active vibration control (one of the possible applications of the system of this work). Although electrodynamic actuators are the cheapest and most common, there is a growing need for alternatives, like magnetostrictive, hydraulic and piezoelectric actuators. A commercial attractive alternative to the traditional voice-coil motors is the more efficient Dielectric Electro Active Polymers (DEAP) technology of the Danish company Danfoss[2], which can be used for actuation, sensing and energy harvesting. However, contact with the company showed that the delivered stroke of their InLastor® Push element is still not enough for this application. It is plausible that in some years, DEAP actuators can be placed in this kind of loudspeaker designs.

For the present design, the driving mechanism is chosen to be 5 BEI LA18-12-000A linear actuators. Each of them provide a peak force of 44.5 N (in total 222.5 N, enough to lift a weight of more than 20 kg), with a maximum

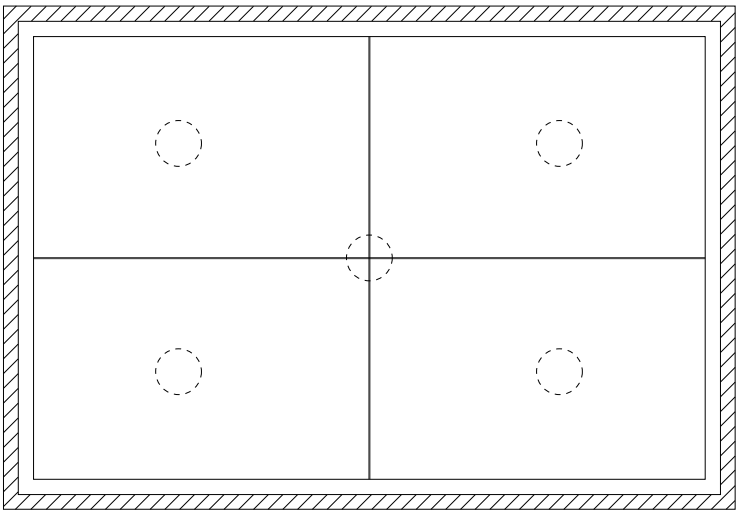

Figure 4.1: *Schematic configuration of the generator, constructed out of 4 A4 pages*

stroke of 3 mm in both sides. The DC resistance is 2.6 Ω which results, for a parallel configuration, in 0.52 Ω. The datasheet of the actuators can be found in Appendix A.

4.3 Suspension

The suspension of the system has to meet some requirements. It forms, together with the actuators, the connection of the radiation plate and the "fixed world". When taking the z-direction as the out-of-plane axis (normal to the plate), the suspension system hast to constrain the panel of moving in the x- and y- axes, while being highly compliant in bending direction. Furthermore, it has to keep the plate in its equilibrium position, independent on the position of the z-axis with respect to the gravitational force (imagine if the loudspeaker is placed on the floor, hanging unther the ceiling or in a wall). With equilibrium position it is meant the position where the electromagnet in the voice coil is ad mid stroke with respect to the magnet. A more detailed discussion of suspension systems is given by van Ophem in [43].

In addition, the volume of air inside the box has to be confined for radiation purposes, to obtain a closed volume. For the prototype, conventional rubber is found to suffice quite well to the constraints. Other methods involving springs and high compliant metal strips are studied, but for practical reasons, the rubber sealing will also be applied for the bigger device. Since the weight of the system can play a role in the fatigue of the rubber, the plate has to be held in its equilibrium position externally. Different methods to achieve this are studied, like the use of a DC current through the coils, or conventional springs inside the enclosure. However, due to DC heat in the coils and ease of montage, it is chosen for external metallic stripes acting as blade springs. With this method, the system can handle changes in the direction of the gravitational field, like

putting the radiator in "vertical" position, when the gravitational force acts perpendicular to z- axis.

4.4 Building of the device

The device is build using the next materials:

- Upper plate: 0.5 mm ST 150 aluminium
- Core structure: aluminium honeycomb 0.2 mm thick
- Lower plate: 0.3 mm stainless steel, with perforation ratio about 54 %. The holes have 5 mm diameter.

The structure was glued together using Araldite 2011, a two component epoxy paste adhesive[1]. The total size is 605x415x22 mm. De size is chosen for con-

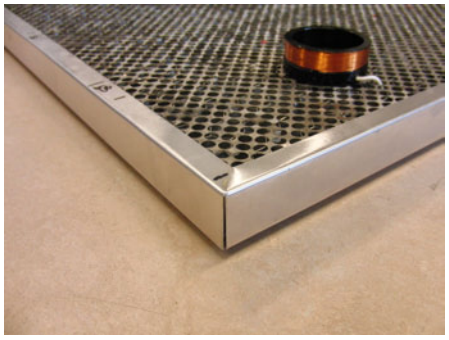

Figure 4.2: *Detail of plate edges*

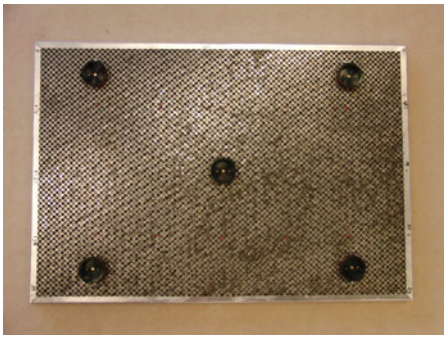

Figure 4.3: *Position of the coils*

venience, since, as explained before, the laser cutting machine (with which the holes are made) can not handle larger structures. For strengthening the edges, a folded 0.5 aluminium U-shape frame is used (as can be seen in Figure 4.2), glued to the structure with Araldite Rapid. The overlap of the frame with the

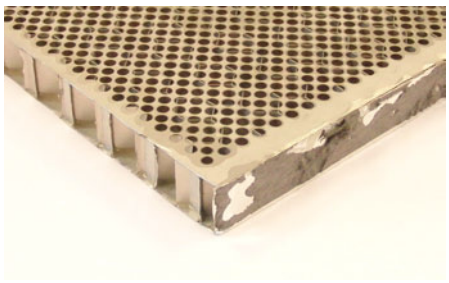

Figure 4.4: *Perforated plate in the structure*

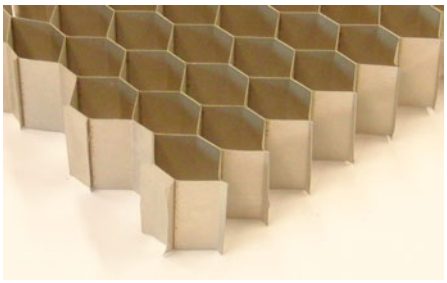

Figure 4.5: *Detail of aluminium honeycomb*

structure is 1 cm. The total weight of the structure is 1112 g. A detail of the

[1]Technical data can be found at `http://www.intertronics.co.uk/data/ara2011.pdf`

backplate in the structure can be found in Figure 4.4. Figure 4.5 shows a close view of the honeycomb architecture.

After that, the coils are screwed to the plate in the positions as shown in Figure 4.3 (following the analysis of Section 5.1). A detailed view of the coil attached to the plate is given in Figure 4.6. On the radiator side, only the head of the fixing screw is visible, as shown in Figure 4.7.

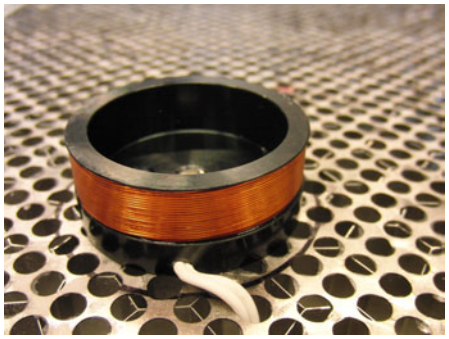

Figure 4.6: *Coil attached to the back of plate*

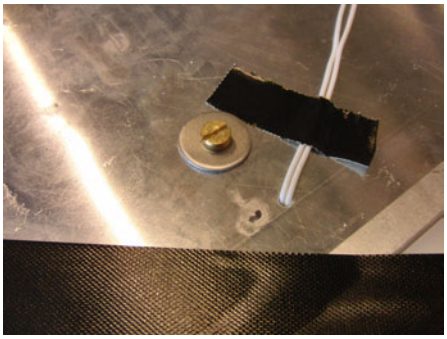

Figure 4.7: *Coil screw and cable in front side of the panel*

The loudspeaker enclosure is made of 20 mm thick Perspex. In the backplate, 5 holes are made to place the permanent magnets. These are screwed on smaller plates, as can be seen in Figure 4.8, to allow fine tuning of their position with respect to the fixed coils. The air cavity is isolated by means of conventional rubber, as explained above. The rubber is attached to the panel and to the enclosure by means of double-sided tape. Figure 4.9 shows the back side of the panel, equipped with the 5 actuators.

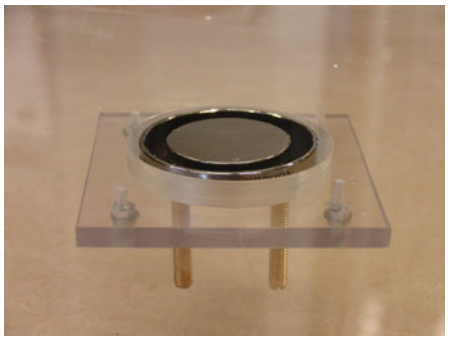

Figure 4.8: *Front view of the magnet with tuning plate*

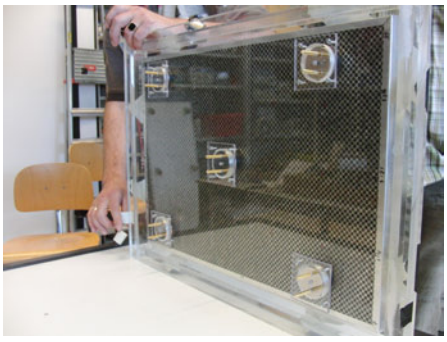

Figure 4.9: *Back view of the panel, with the five magnets*

As finishing touch, two reinforcing ribs are placed on longest side of the back plate of the enclosure, to avoid the formation of vibration patterns which can influence the quality of the radiated sound. The radiating plate is then suspended on its equilibrium position by four RVS stripes (2 mm thick, 1 cm

wide) acting as external blade springs. Both additions can be seen in Figure 4.10. Figure 4.10 also shows the isolation layer from the external medium to get reliable measurements.

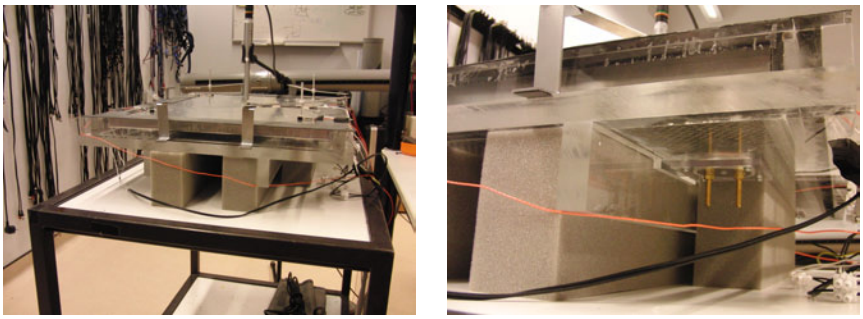

(a) *Overview*

(b) *Detail of the back side*

Figure 4.10: *Flat loudspeaker, finished*

Chapter 5

Practical validation

In this chapter, the experimental setups used for the practical validation of the sound generator are discussed. In the first place, the mechanical vibration research method is outlined. After that, the measurement of the acoustical and electrical quantities will be presented.

5.1 Mechanical validation

As outlined in one of the previous chapters, an externally excited panel will vibrate with a set of patterns, called structural modes, which will depend on the frequency of the external source, the place of the excitation and the dimensions and mechanical characteristics of the panel. Measuring of this excitation patterns is essential for understanding the dynamic behaviour of the panel. In this section, the measurement techniques and the experimental results of this so-called modal-analysis will be presented. In this analysis, the Frequency Response Function (FRF) of the plate will be computed from the response (acceleration/velocity/displacement) to a known excitation (mechanical force). Measurements are performed for two situations. In the first place, only the plate will be studied, hanging freely in the space. After that, the plate will be placed in the enclosure, and the measurements will be repeated. In this case, the air layer behind the plate is expected to play a major role. This last experiment will be extended by placing 5 weights on the plate, simulating the part of the actuators which is attached to it.

5.1.1 Experimental setup

As discussed in previous sections, the total frequency response of the plate is given by

$$FRF = \sum_{i,j}^{M,N} H_{ij} \tag{5.1}$$

where, after discretization of the two dimensional plate in M x N discrete points (called node points), H_{ij} is the response of point j to an excitation at point i. The resolution needed depends on the frequency region of the measurements. In this project, it is chosen for $M = 7$ and $N = 5$, which results in a total of

35 points. Given the size of the plate, 10 cm distance between adjacent points seems reasonable for measurements below 800 Hz. To get the total frequency response function of the plate, the response of each point to an excitation in each other point has to be measured. However, for 35 points, this would result in 1225 measurements times the number of averages per point. However, since the system is assumed to be linear, this number can be drastically reduced. If for instance the responses of points 2 and 3 to an excitation at point 1 are measured, the response of point 3 to an excitation at point 2 can be computed. Extending this reasoning to the whole set of points, it can be concluded that the whole system can be characterized by excitation at one single point and measurement on all the other points (or inversely, measurement at one point to excitations at all the other points). However, the choice of the single excitation of measurement point has to be carefully made: There are modes which are not (or difficult) excited at some given points and, conversely, there are points which remain still for a given mode. For this reason, it is a safer option to measure (or excite) at two points, even if that introduces redundancy in the measurements.

Two main excitation techniques are considered. On the one hand the impact hammer, which is a specially prepared hammer with a force sensor on the tip. The structure is excited at each point, and the response is measured at two (to be sure all modes are measured, according to the discussion above) different fixed points of the structure. On the other hand, the structure can be excited at one specific point by means of an electromechanical shaker with a force sensor between the shaker and the structure. The shaker can be fed with a random or a chirp signal, and measurements are done on all points of the structure. To make sure all modes are excited, the process is repeated with the shaker placed at a different node point. The hammer hit has a relatively flat energy spectrum up to around 1 kHz, which makes it suitable for studies under this frequency. However, when a different spectrum is needed, or when the hit could damage the structure, the less flexible shaker excitation method can be used.

After measuring the excitation force and the response, the FRF can be computed, usually as the quotient between the cross power spectrum of the response and the input force and the auto power spectrum of the force. The coherence of the measurement is defined as

$$\gamma^2 = \frac{|G_{XF}|^2}{G_{XX}G_{FF}} \tag{5.2}$$

where G stands for a power spectrum. The coherence is a measure for the quality of the measurement.

For analysing the data, a '3D wire frame model' with 35 node points built in the Modal/Structural Analysis program ME'scope is used, as can be seen in Figure 5.1. The data acquired by the DSP Siglab and processed in the PC by Matlab are imported within this frame for visualising and further calculations. Other equipment used for this study is:

- Impact hammer: Brüel & Kjær (B & K) 8202 / force sensor B & K 8200
- Exciter: B & K 4809/ force sensor B & K 8001

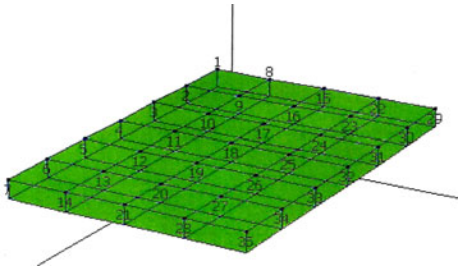

Figure 5.1: *Structure in ME'scope with labelled node points*

- Accelerometer: B & K 4517
- Calibration Exciter: B & K 4294
- Signal amplifier: B & K NEXUS
- (Shaker) power amplifier: B & K 2706
- DSP: SigLab 4-channel Model 20-42
- Structural Analysis software: MEscope

5.1.2 Measurement results

The first study is about the independent or "uncoupled" system. For this pur-

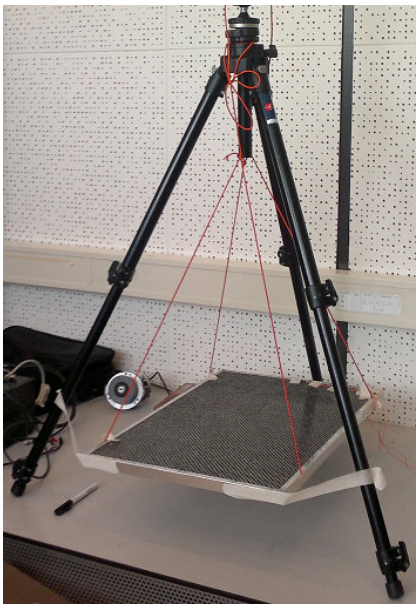

Figure 5.2: *Setup for uncoupled structural measurements*

pose, the plate is suspended by high elastic springs, in order to lower the rigid body modi frequencies to make sure they not interfere with the eigenfrequencies

of the system. The setup built can be seen in Figure 5.2.

The plate is then excited with a hammer (as can be seen in the detailed picture of the setup, Figure 5.3), and the responses are measured with Siglab. The average of three hits is taken for every node point, to reduce the measure-

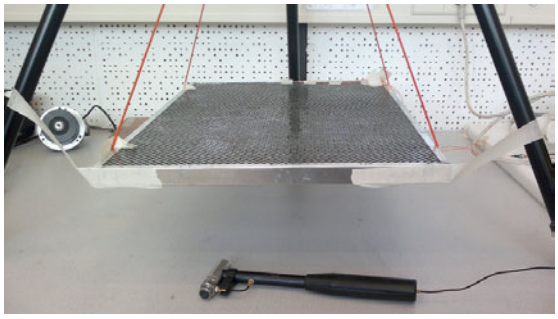

Figure 5.3: *Detail of the setup, with excitation hammer*

ment error. Every hit is triggered and, in order to make sure that the whole signal is taken into account, a delay of one second is applied. The values of the signal amplifier are introduced in Siglab to get results in real units. The measuring is taken in the highest accuracy possible, 13 bits, and the resulting signal is filtered with an exponential filter, which makes sure only the first 20% of the force signal is taken into account. Furthermore, the overload signals are rejected. With this settings, an eigenfrequency analysis was performed, below 1kHz. As expected, all rigid body modi are in the region under 10 Hz. Figure 5.4 shows the vibration modes of the first six eigenfrequencies of the plate. In

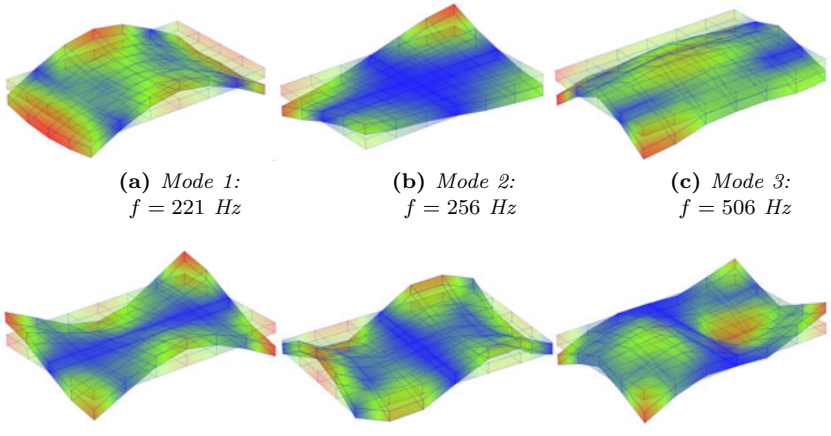

(a) *Mode 1:* $f = 221$ *Hz*
(b) *Mode 2:* $f = 256$ *Hz*
(c) *Mode 3:* $f = 506$ *Hz*
(d) *Mode 4:* $f = 571$ *Hz*
(e) *Mode 5:* $f = 611$ *Hz*
(f) *Mode 6:* $f = 775$ *Hz*

Figure 5.4: *Structural modes of uncoupled plate*

this case, no viscous damping affects the system. Only the effect of structural damping can be seen.

After that, the structure is placed in the enclosure, about 9 mm above a hard panel, attached to a fixed levee by means of conventional rubber, allowing it to

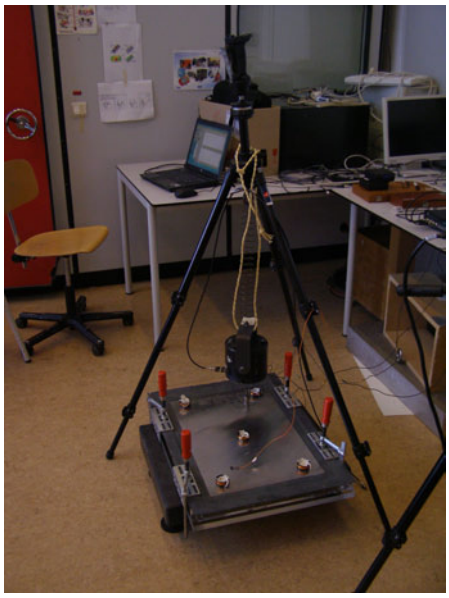

Figure 5.5: *Setup for shaker measurements*

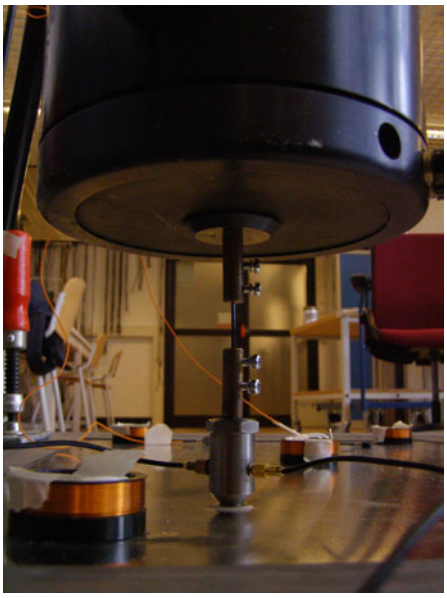

Figure 5.6: *Detail of rigid connection to the plate*

move relatively free in the 'z direction' (the smallest dimension of the panel), but confining the air to stay inside the cavity. A modal analysis of this new "coupled" system is performed with Siglab. In this case, the excitation is done by means of a shaker, fixed at points 23 and 24 in Figure 5.1. Figure 5.5 shows

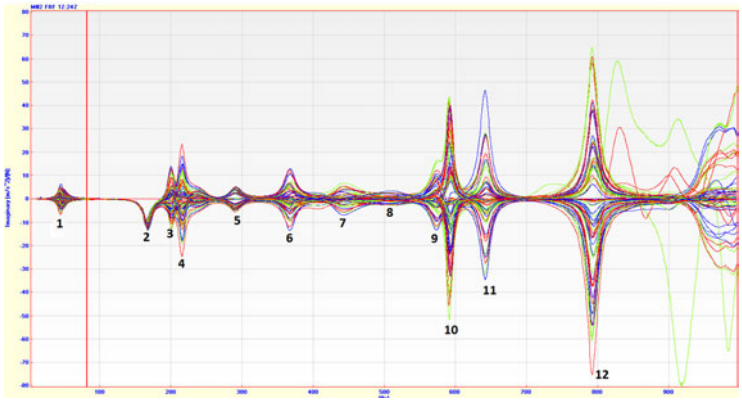

Figure 5.7: *Imaginary part of the frequency response function of all points for shaker measurements*

the setup of the measurements and the way the shaker is suspended above the panel. Figure 5.6 shows a detailed view of the shaker attached to the panel and the force and acceleration sensors on the tip. The excitation by the shaker is chosen to be a random signal with 1 kHz bandwidth. The signal is averaged

to 20 measurements, with an overlap of 50 %. Figure 5.7 shows the imaginary part of the FRF below 1 kHz.

In a plot of the imaginary part of a response function, like the one shown in 5.7 (where the responses of all points to the two excitation points are displayed), it can be seen of the motion of the measurement point is in phase or counterphase with respect to the excitation point. For instance, it can be deduced that the point 2 in Figure 5.7 corresponds to the rigid body mode where all shapes move in phase. In this analysis, some of the rigid body modes can be identified at higher frequencies than in the uncoupled case (as expected), due to the stiffness of the air layer. Three of them can be seen in Figure 5.8 (the numbers correspond to the shape in Figure 5.7, not to the mode number). The first two structural

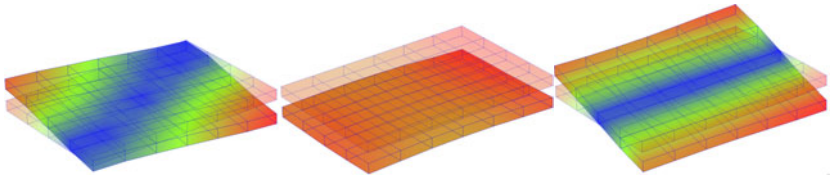

(a) *Point 1:* $f = 46$ *Hz*
(b) *Point 2:* $f = 168$ *Hz*
(c) *Point 5:* $f = 291$ *Hz*

Figure 5.8: *Rigid body modes of the coupled plate*

vibration modes are also easily recognisable, at slightly lower frequencies than in the coupled case (they are labelled 3 and 4 in Figure 5.7). The next four modes (9, 10, 11 and 12 in Figure 5.7) can be found at higher frequencies in the coupled system, as shown in Figure 5.9, with respect to the uncoupled case (compare Figures 5.4 modes 3, 4, 5 and 6 respectively). This could be caused by the acoustic modes in the system, which couple better at those frequencies. Two things are remarkable: First, the fact that the two first modes are switched

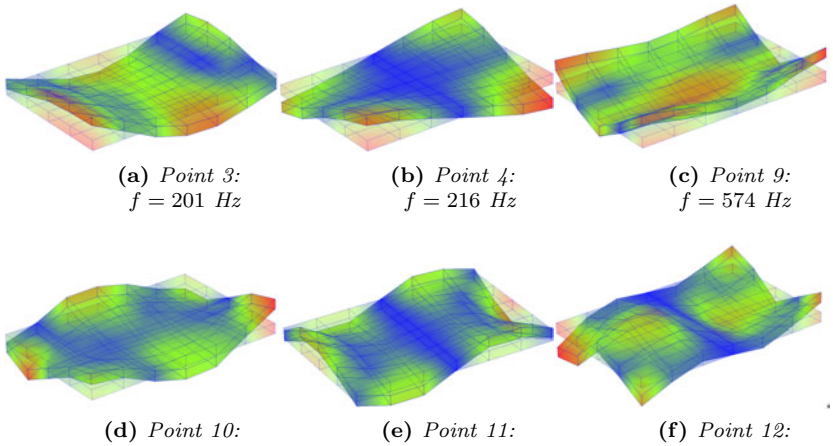

(a) *Point 3:* $f = 201$ *Hz*
(b) *Point 4:* $f = 216$ *Hz*
(c) *Point 9:* $f = 574$ *Hz*
(d) *Point 10:* $f = 592$ *Hz*
(e) *Point 11:* $f = 643$ *Hz*
(f) *Point 12:* $f = 793$ *Hz*

Figure 5.9: *Vibration modes of the coupled plate*

with respect to the simulations in Figure 3.5. This shows the invalidity of the assumptions made to generate the comsol simulations. Second, the mode in Figure 5.10: It presents exact the same shape as the 2nd mode, with slightly lower amplitude. The orthotropic character of the honeycomb in combination with the air layer could explain this effect: the torsion modes in both transversal directions seem to be decoupled.

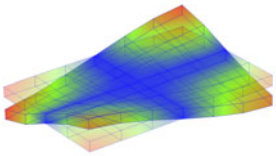

Figure 5.10: *Point 6 of the coupled plate.* $f = 368$

For completeness, the patterns corresponding to peaks 7 and 8 in Figure 5.7 are shown in Figure 5.11. The amplitudes of these modes are much lower than the principal modes of Figure 5.9 (note that in the figures presented in this section, the maxima and minima are normalized per figure. The real scale of the vibration amplitudes can be found in a graph of all modes, like Figure 5.7). After

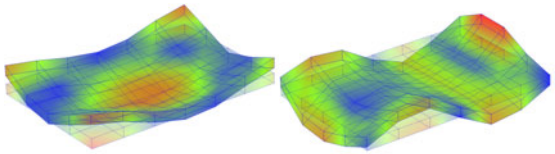

(a) *Point 7:* $f = 443$ *Hz*

(b) *Point 8:* $f = 510$ *Hz (very weak mode)*

Figure 5.11: *Vibration modes of the coupled plate*

that, the measurement is repeated with five weights added to the structure to simulate the electromagnets. As expected, the resonance frequencies are lower than when the plate is free. The frequency changes are summarized in the next table:

	f (no weights)	f (with weights)
Rigid Body modes	46	42
	168	152
	291	286
Vibration modes	201	195
	216	200
	368	354
	574	568
	643	639
	793	782

In Figures 5.8, 5.9 and 5.10 can be seen that, even when the plate is suspended in the cavity, the rubber is compliant enough to allow the ends of the plate to move freely (as if they are not supported). In the first bending mode, at 201 Hz, the center and the sides show the highest displacement, whilst in first torsion mode, at 216 Hz, the displacement of the coners is the most promiment. This means that by supporting the center and the corners, the tendence of the plate to eigen vibrations will be reduced the most (for the lowest frequencies). Therefore, the positions of the five actuators is chosen to be one at the center and the other 4 each close to one corner.

5.2 Electroacoustical validation

In order to fully describe the loudspeaker behaviour, some of the quantities discussed in Section 2 are measured. In this section, the measurement method for these quantities is discussed and the results are presented. In all measurements, the performances of the feedback and feedforward control are compared. The measurements are performed in Matlab Simulink version 7.8.0 (R2009a). Other equipment used includes

- Measurement microphone: Behringer ECM8000 condenser microphone
- Microphone calibrator: Tenma 72-7260, 94 dB $\pm$ 0.8 dB at 1 kHz $\pm$ 5 %
- Microphone amplifier: Tascam MA-8 Calibrated to produce 2V output for 94 dB at 1 kHz
- Accelerometer: B & K Deltatron Accelerometer Type 4517 - 002
- Accelerometer amplifier: Voltage amplifier designed by H. Huipers, SAS group, University of Twente. It is calibrated to deliver 100 mV/g = 10.2 mV/m/s^2. A schematic of the accelerometer amplifier can be found in Appendix B.
- Driver amplifier: Current amplifier designed by H. Kuipers, SAS group, University of Twente. Delivers a constant current of 1 A/V. A schematic of the driver amplifier can be found in Appendix C.
- Platform: Real time Simulink development platform with Xenomai Linux OS. More information on the platform can be found in the next section.

The accelerometers are calibrated at 100 Hz. A constant sine signal is generated, and the output is (externally) measured to be 85 mV_{pp}. The value inside the platform is 33.5 mV_{pp}, which means that if the accelerometer signal (in Volt) is multiplied by a factor of 2.54/100, the value in g is obtained. Therefore, multipying the accelerometer signal by a factor 0.25 (9.8*2.54/100) yields the value of the acceleration in m/s^2, assuming a flat linear accelerometer response. Using a similar reasoning, for the microphone, yields a correction factor equal to 3.53 to convert to a 94 dB scale, or 0.0375 to get the result in dB.

5.2.1 Real time development platform

The development platform is fully described by Wesselink in [45]. Figure 5.12 shows a schema of the signal processing part of one of the 16 channels occurring inside a 100 kHz FPGA. It consists of 2 paths: The first one (low authority) goes through three programmable IIR filters and a gain block (which can be placed in each of the 4 positions relative to the filters: preceding the first filter, between the first and the second, etc), before being added to the high authority path, the Simulink core. Before going to the core, which operates with lower sample frequency (in this project, 10 kHz), the signals are downsampled by means of a two stage decimator. After the Simulink process, the signals are interpolated again. The two paths are added together and go through a last optional IIR filter, which will be used in this project for the feedforward control. However, using this filter in the same channel as the feedback control would include it in the feedback loop. The solution is to use a different channel (with everything else disabled) to implement the IIR filter: The output of the "processing" channel will be directly connected to the input of this channel and the output will be taken as overall output.

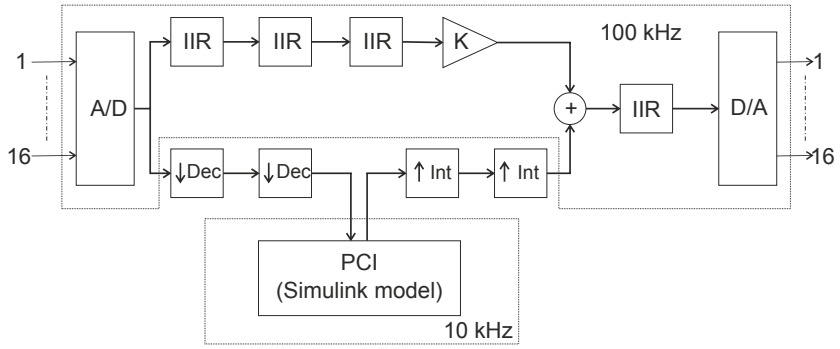

Figure 5.12: *FPGA Signal processing path*

The response of the two stage decimation step is shown in Figure 5.13. Both filters are designed as 60 taps FIR filters, the first one with a (normalized) cut off frequency of 0.5. For the second one, this frequency is 0.2.

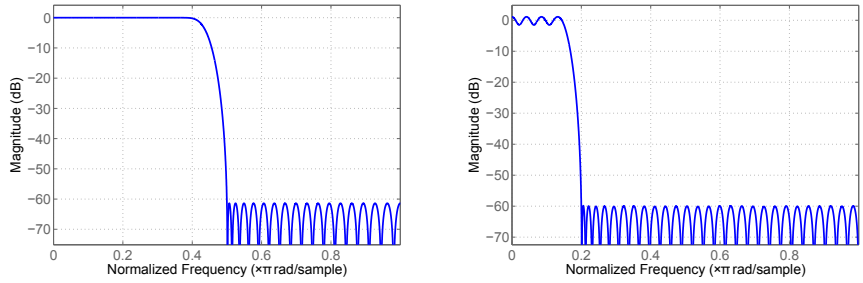

(a) *100 kHz to 20 kHz* **(b)** *20 kHz to 10 kHz*

Figure 5.13: *Two-stage decimation step: 100 kHz to 10 kHz*

Figure 5.14 shows the response of the interpolation filters. These filters are also designed as FIR filters. The first one, with a factor 2 interpolation frequency, is a 60 taps filter, and the second one, with a conversion factor of 5, is implemented with 127 taps.

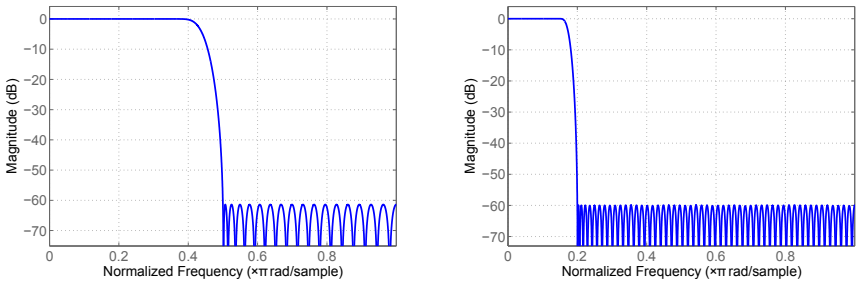

(a) *10 kHz to 20 kHz* **(b)** *20 kHz to 100 kHz*

Figure 5.14: *Two-stage interpolation step: 10 kHz to 100 kHz*

One of the advantages of the platform is the possibility of performing calculations in the FPGA, with a higher sample frequency. In this project, the low authority path (in the FPGA) will be used to integrate the acceleration, used in the velocity feedback control. The first stage of the integrator is used to filter out DC components. The second filter is the actual integrator, a low-pass filter with 10 Hz as corner frequency, and the third stage is used to filter out the undesired high frequencies above 1 kHz. The gain block is placed after the three filters, to avoid too much signal looses in the filtering process. Its value is set to -50 (negative feedback). Figure 5.15 shows the response of the integrator measured with Siglab. It can be seen that the response decays with -6 dB per octave, from the corner frequency, around 10 Hz.

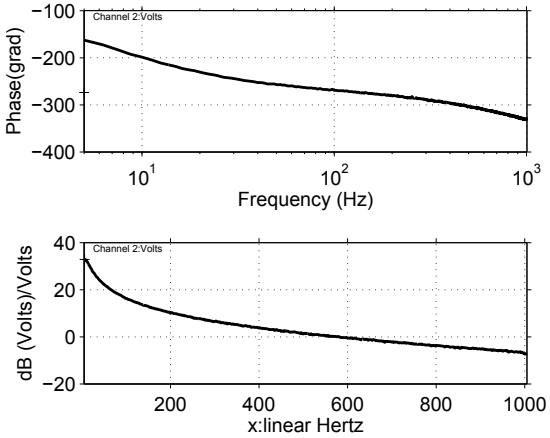

Figure 5.15: *Integrator response*

The feedforward control filter response (as measured with Siglab) is shown

in Figure 5.16. As can be seen, a HPF is also implemented in the filter path, to protect the system from undesired DC components. The filter shows a strong amplification in the range 0.5-80 Hz, which is the region of interest for feedforward correction.

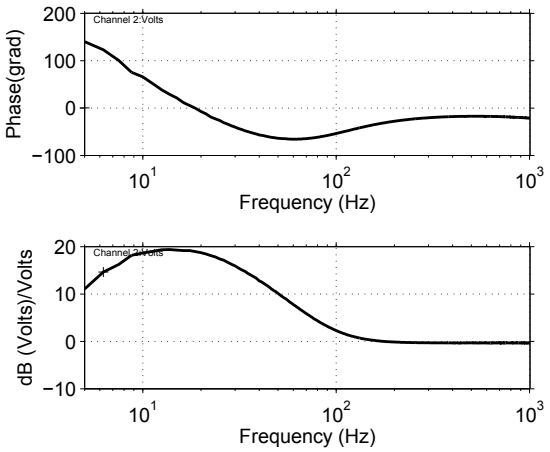

Figure 5.16: *Integrator response*

The Simulink model used is shown in Figure 5.17. As can be seen, there are three blocks which interact with the "outside" world. The first block, `Enable_Sysid`, enables the (generated) input signal used. Up to this point, three different input signals have been used: A sine wave, for calibration purposes, and a chirp and a random signals for measurements. This signal is filtered

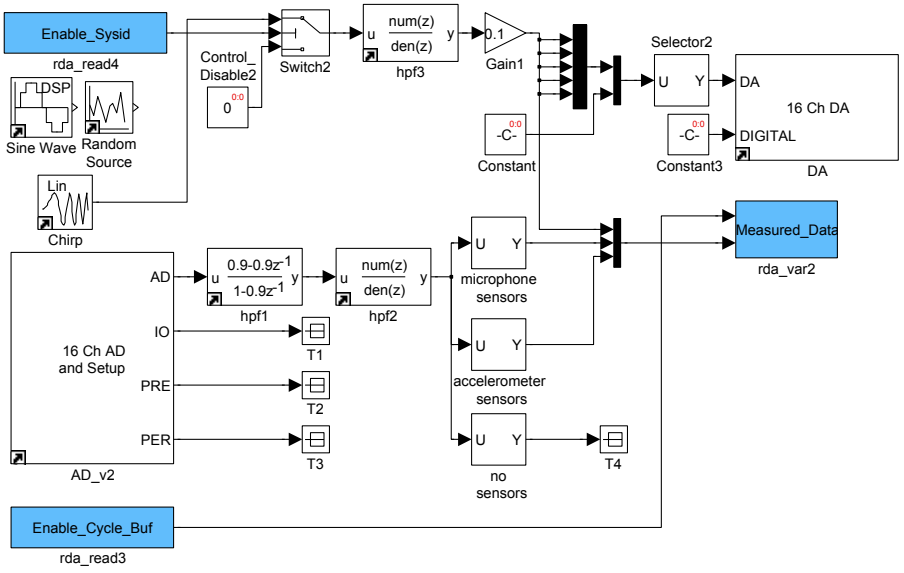

Figure 5.17: *Simulink model*

in `hpf3` to avoid undesired DC components. The second communication block, `Enable_Cycle_Buf`, regulates the writing of the cyclic buffer, which can be read by means of the `Measured_Data` block. In the case represented in Figure 5.17, the inputs of the cyclic buffer are the input signal (before going to the D/A convertor), and the input signals, microphone and accelerometer, coming from the A/D convertor. The input signals are also filtered to avoid the presence of DC components. In this work, to avoid undesired effects of the filters, `hpf1`, `hpf2` and `hpf3` are left as wires (their transfer function is set to 1).

5.2.2 Setup of the measurements

Due to the fact that stability is not guaranteed when controlling de actuators independently, possibly due to the fact that the sensor-actuator combinations are not independent and influence each other (in a way such that factor G in Equation 2.78 is not positive definite), the measurements done in this section are performed in a configuration where a single signal is generated by the platform and is distributed to the actuators in parallel. This means that there is only one integrator and one feedforward corrector implemented. Unless specified, the sensor used for the feedback signal is located in one of the corners. As will be shown below, in Section 5.2.11, instability arises when the feedback gain is higher than -8. However, for this value, the effect of the active damping is barely seen. In the subsequent sections, the measurement results for two values of the feedback gain will be presented: one where $K = -8$ and stability is guaranteed, and one where $K = -70$, and the effect of the control is well appreciated. The input used is a chirp signal which varies linearly from 30 Hz to 1 kHz. For the analysis of the measurements, only full periods of the signals are taken, to have uniform representation of all frequency components.

5.2.3 Thiele/Small parameters

The small signal Thiele/Small parameters for low frequency behaviour are, as described in Section 2.2.2, f_s, V_{as}, Q_{es} and Q_{ms}, measured by low signal. f_s can be directly extracted from the frequency measurements, it is the (lowest) resonance frequency of the driver. The value of V_{as} can be easily computed with

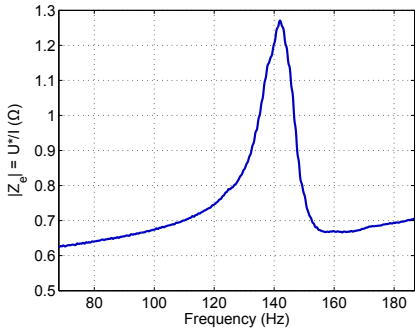

Figure 5.18: *Impedance peak*

the known volume of the enclosure at maximum excursion. The quality factor

Q is defined as the -3dB bandwidth divided by the resonance frequency, which can be seen in Figure 5.18 (however, the values can not be extracted from there, due to a wrong scale, as will be discussed later). According to a -6dB method, the values of Q_{es} and Q_{ms} can be defined as

$$Q_{ms} = f_s \sqrt{\frac{r_0}{f_h - f_l}} \tag{5.3}$$

$$Q_{es} = \frac{Q_{ms}}{r_0 - 1} \frac{R_e}{R_s + R_e} \tag{5.4}$$

where r_0 is a reference value introduced by Small, defined as the ratio of the current set (nominal current in the linear region of the loudspeaker) to the current at resonance frequency, and f_h and f_l are the -6 dB frequencies. R_e is the electric resistance of the speaker, and R_s is a measuring resistance. For the subject of this study, this leads to the following values (the dimensionless r_0 is measured to be 0.6811):

$$f_s = 142 \text{ Hz} \tag{5.5}$$

$$V_{as} = 14.75 \text{ litres} \tag{5.6}$$

$$Q_{ms} = 37 \tag{5.7}$$

$$Q_{es} = 106 \tag{5.8}$$

$$Q_{ts} = 27.46 \tag{5.9}$$

As will be shown for in the comparison with a conventional loudspeaker, the values for the Q factors are really high. This fact is explained by the high resonance frequency and the sharpness of the peak (low damping).

5.2.4 Frequency response function

As illustration, the first graphic presented in this report corresponds to the FRF, using a chirp signal as input, and a pressure microphone suspended 2 cm

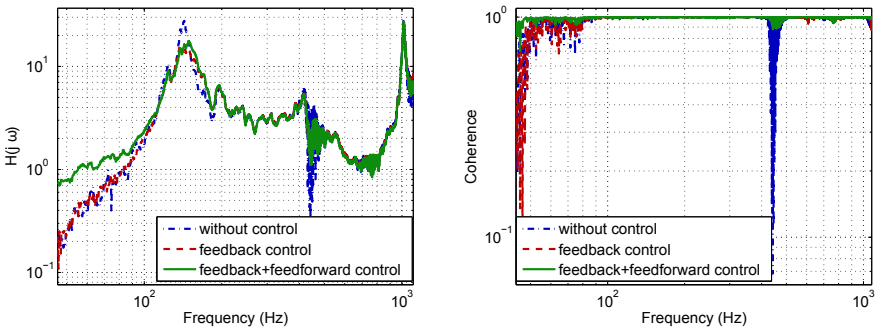

(a) *Transfer function* **(b)** *Coherence*

Figure 5.19: *FRF. Input: Chirp signal (30-1000Hz). Output: Pressure microphone signal. Feedback control* $K = -8$

above the panel as output. The FRF is computed as

$$H(j\omega) = \frac{S_{II}}{S_{IO}} \tag{5.10}$$

where S_{II} is the auto spectral function of the input and S_{IO} is the cross spectrum of the input and output. Figure 5.19 and 5.19 show the transfer function and the coherence function for the case $k = -8$ and $K = -70$ respectively. They

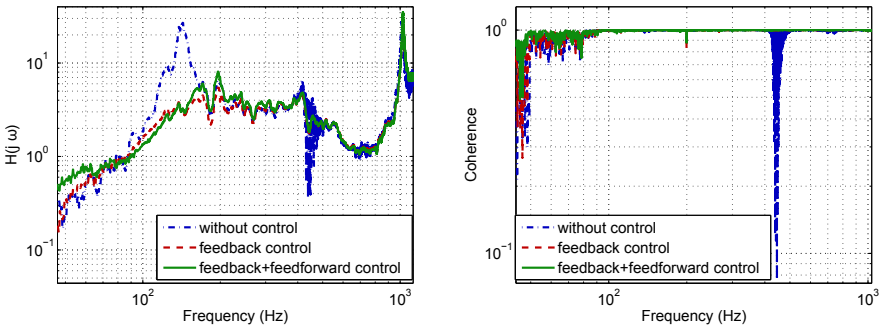

(a) *Transfer function* **(b)** *Coherence*

Figure 5.20: *FRF. Input: Chirp signal (30-1000Hz). Output: Pressure microphone signal. Feedback control* $K = -70$

show some general aspects of the driver, like the resonance frequency of the plate, around 140 Hz, and two other resonance peaks, around 410 Hz and 1kHz. The working of the correction is also proved, especially in Figure 5.20. With only feedback control, the response is flattened, and a second filter extends the frequency response in the low frequencies. However, the effect of this filter is only seen for really low frequencies around 40 Hz. This fact can be explained by the fact that the low frequencies correction filter is designed for a loudspeaker with second order response, and the subject of this study is clearly of higher order. A higher order filter would improve the response of he low frequencies as desired. In Figures 5.19 and 5.19, the coherence of the measurements is shown, proving their validity.

5.2.5 Electrical impedance

The electrical impedance of one actuator of the loudspeaker is given by (now assuming steady state behaviour)

$$Z_{vc}(j\omega) = \frac{u(j\omega)}{i(j\omega)} \tag{5.11}$$

Note that the expression for Z_{vc} in Equation 5.11 is the transfer function from an imput current to an output voltage. Therefore, the Matlab function `tfestimate` can be used to extract the electrical impedance from the current and voltage time measurements, where the voltage over the coil is measured directly, and for the current the voltage over a series resistor ($R = 0.337$) is taken. Special attention has to be given to the measuring resistor: Its value has to be subtracted from the real part of the total electrical impedance. The total impedance is computed given the parallel configuration of the actuators, as

$$\frac{1}{Z_{vc}(j\omega)} = \sum_{i=1}^{N_{actuators}} \frac{1}{Z_{vc,i}(j\omega)} \tag{5.12}$$

where $Z_{vc,i}$ is the impedance of the ith actuator. Figure 5.21 shows the total

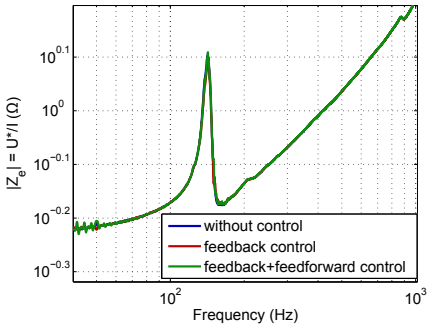

Figure 5.21: *Electrical impedance of the driver*

electrical impedance of the driver. The resonance peak at 142 Hz, where the impedance is merely real, is clearly seen. It also shows that the capacitive working of the speaker is in a really short frequency range: After around 160 Hz, it shows a clearly inductive tendence. Furthermore, in Figure 5.21 can be seen that the impedance is a characteristic of the circuit and therefore does not change by applying correction filters.

5.2.6 Acoustic impedance

Since the acoustic impedance of the loudspeaker inside the enclosure is the quantity of interest and with the present configuration only the impedance outside could be measured (which would be a grosso modo the impedance of air), measuring of the acoustic impedance will be skipped.

5.2.7 SPL halfspace at 1 meter distance

The first approach for displaying the SPL halfspace is to measure the nearfield pressure with the microphone and apply a correction factor

$$\frac{S_d}{2\pi r} \tag{5.13}$$

as discussed in Section 2.2.5. However, due to the dimensions of the speaker, it is not reliable to assume that 1 meter corresponds to a point in the farfield. For this reason, the method chosen in this work is to extract the particle velocity from the plate acceleration (by a simple integration) and use the Rayleigh integral as in Equation 2.50 to compute the SPL halfspace at 1 meter distance (for the case the system is assumed to be placed in an infinite baffle). Figure 5.22 shows the SPL halfspace at 1 meter distance obtained with this method for two values of the feedback gain. The corresponding input power will be discussed in the next section. For now, the SPL is not corrected for any weighting curve.

The SPL shows the expected response: It presents a high peak at resonance, which is flattened with the feedback control (especially in the case where the feedback control gain is -70). The subtle work of the correction filter can also

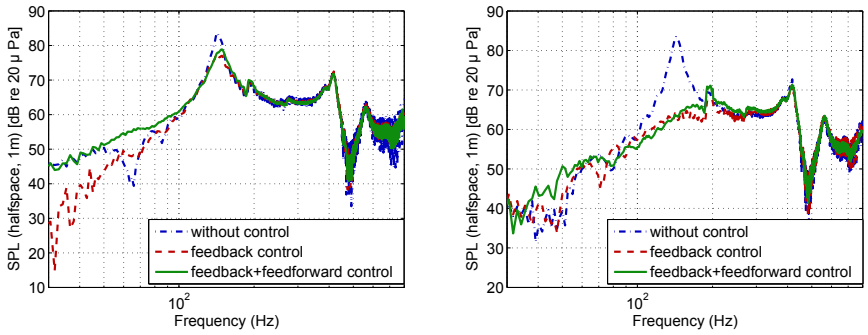

(a) $K = -8$ **(b)** $K = -70$

Figure 5.22: *SPL halfspace at 1 meter distance*

be noticed in the low frequencies. For the given power, it has a value of around 65 dB in the "flat zone". In the next section, the power corresponding to this value is presented.

5.2.8 Electric input power

The SPL computed in the last section is a quantity which depends on the electric input power, which is easily computed from the voltage over and the current through the coil in the frequency domain as

$$P_e = \frac{1}{2}\mathcal{RE}\{U^*(j\omega)I(j\omega)\} = \frac{1}{2}\mathcal{RE}\{U(j\omega)I^*(j\omega)\} \tag{5.14}$$

where $\{\cdot\}^*$ denotes the complex conjugate and $\mathcal{RE}\{\cdot\}$ the real part of the quantity within brackets. Both the voltage and the current were measured for the input impedance, and will be used again to compute the electric power. The total power of the actuator is simply the sum of the power dissipated by each of the actuators, and is shown in Figure 5.23. As expected, the power of the

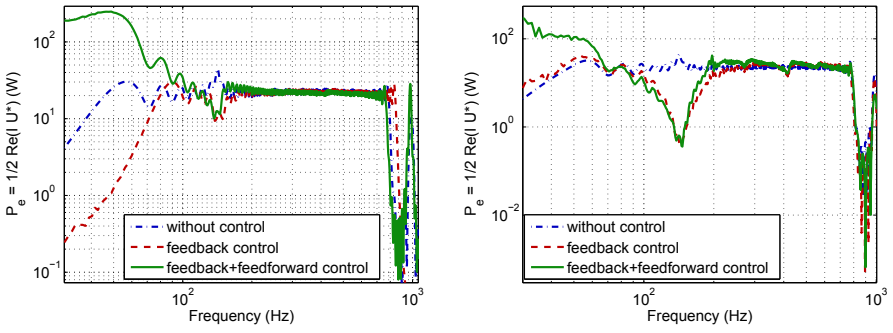

(a) $K = -8$ **(b)** $K = -70$

Figure 5.23: *Total electric power of the driver*

controlled system experiences a drop at the frequency of resonance, since much

less energy has to be delivered to the system in that region. It can also be seen that a lot of power has to be pumped in the system to extend the low frequencies region by means of a feedforward filter. As discussed in the previous section, a more suitable quantity to describe loudspeaker behaviour is the SPL at 1 meter distance corresponding to an input power of 1 Watt. It can be seen in Figure 5.23 that in the "flat region" (from 200 Hz to 800 Hz), the electric power delivered to the system is around 10 Watt. The SPL corresponding to a power of 1 Watt is simply the SPL found above minus 10 dB. In this case, it can be stated that the SPL corresponding to 1 Watt, delivered to halfspace at 1 meter distance is 55 dB.

5.2.9 Acoustic power

Analogue to the electric power, the acoustic power can be computed as the product of the pressure and particle velocity, in the frequency domain (with the complex conjugate of one of the two quantities). Both were already computed for the measurements of the acoustic impedance. Figure 5.24 shows the acoustic power of the loudspeaker system.

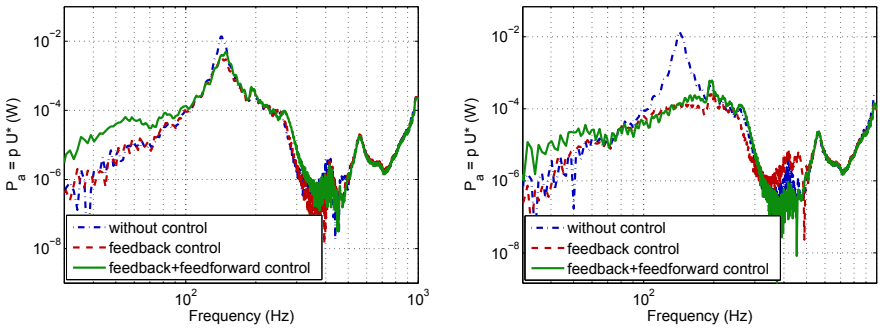

(a) $K = -8$ **(b)** $K = -70$

Figure 5.24: *Acoustic power of the driver*

5.2.10 Efficiency

The efficiency is simply defined as

$$\eta = P_A / P_E \tag{5.15}$$

and can be obtained with the results for the electric and acoustical power. Figure 5.25 shows the efficiency versus frequency of the driver. As expected, the efficiency is high around the resonance frequency. However, the units of the acoustic power (Figure 5.24) are unrealistic. This involves that nothing about absolute or average values of the efficiency can be said with the work done until now.

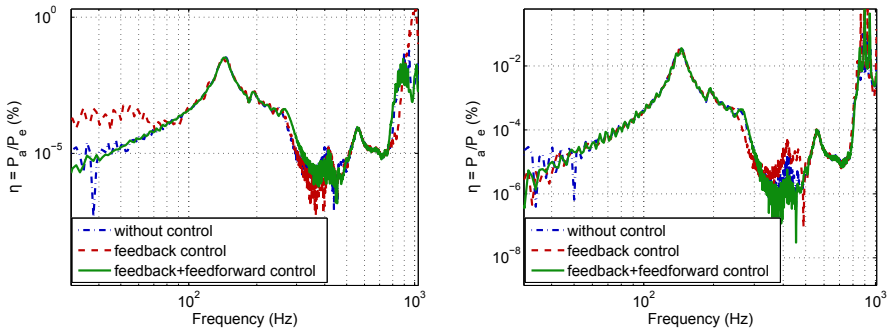

(a) $K = -8$ **(b)** $K = -70$

Figure 5.25: *Efficiency of the driver*

5.2.11 Stability

Following the discussion in Section 2.4.1, the stability of the feedback control loop can be deduced from a Nyquist plot, the real-imaginary plot of the loop gain $L = H(s)D(s)K$, where $H(s)$ is the transfer function from actuator to sensor (force to acceleration), $D(s) = 1/s$ is the integrator (compensator) and K is the value of the feedback gain. The measuring method for this open loop is schematically shown in Figure 5.26. Figure 5.27 shows the Nyquist plot of

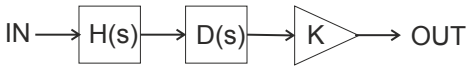

Figure 5.26: *Feedback control open loop*

the feedback control loop used in this project for different gain values. It can be seen that the system becomes unstable (the curve contains the point -1) for values of $K > 8.6$.

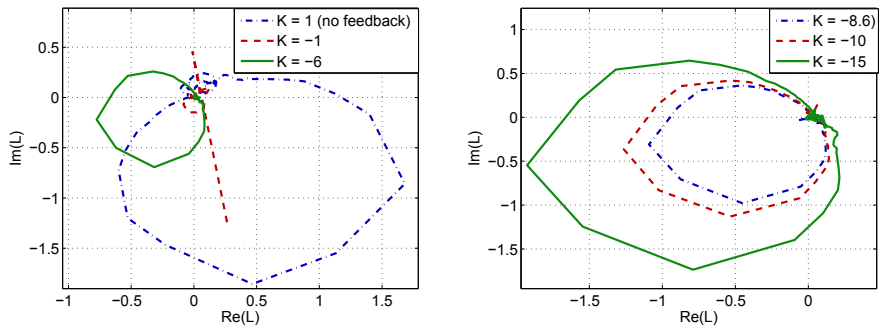

(a) **(b)**

Figure 5.27: *Nyquist plots for different gain factors*

5.3 A conventional driver: A comparison

For comparing the performance of the final product with an existing commercial driver, the JBL P1022 10" woofer is chosen. The datasheet of this driver can be found in Appendix D. The specifications are

- Sensitivity (2.83 V @ 1m): 96 dB
- Frequency response: $25 \approx 500$ Hz
- Nominal impedance: 2 Ω per coil
- Free air resonance $f_s = 29$ Hz
- Mechanical Q-factor: $Q_{ms} = 8.21$
- Electrical Q-factor: $Q_{es} = 0.58$
- Total Q: $Q_{ts} = 0.55$
- Compliance volume $V_{as} = 20$ litres

It can be seen that the overall performance of the designed loudspeaker is lower than that of a conventional loudspeaker. However, the gain in size (flatness) (and weight) is considerable. Furthermore, the frequency response region is much lower compared to existing flat loudspeaker technologies and conventional drivers with the same size (in the direction of motion).

Chapter 6

Conclusions and recommendations

In this chapter, the discussion of the results in the past sections will be summarized. After that, some recommendations for further work will be exposed and elaborated.

6.1 Conclusions

A flat loudspeaker has been successfully built as a flat panel with dimensions 0.605 x 0.405 x 0.02 m. The enclosure has (inside) dimensions 0,635 x 0.435 x 0.05 m, and the radiating panel is held inside the enclosure (as shown in Figure fig:configuration. A conventional rubber edge confines the air inside the enclosure. The plate is held in position by four external aluminium strips acting as blade springs, one in each corner. The loudspeaker is driven by 5 conventional voice-coil actuators, placed one in the center and the other four near the corners, to compensate the "weakest" points of the plate.

The response of the driver has a high resonance frequency at 142 Hz, due to the dimensions of the radiator plate. A correction for this resonance peak is implemented by means of velocity feedback. The response is also extended to the low frequencies thanks to a feedforward correction filter. The implemented correction filter does not perform well in the region immediately before the resonance frequency, only at lower frequencies. This fact can be explained by the fact that the filter is designed for a second order system, and the loudspeaker designed in this project shows higher order behaviour. The performance can be increased by designing a higher order correction filter.

The SPL halfspace at 1 meter distance corresponding to a power of 1 W is 55 dB. It's lower than expected (from the simulations), and lower than the reference driver used.

According to the Nyquist plot, the feedback control becomes unstable for low values of the gain, where the working of the control loop is barely appreciated.

However, measurements with a higher gain result in a flat response, without audible instability.

6.2 Recommendations

Being the system described in this work a first prototype of such loudspeakers, there are many possibilities for further research. Some of them will be discussed here. In the first place, some things can be done on the existing device:

- Modal analysis of the whole system. A new modal analysis could give insight in the influence of the electrical circuit and the external springs in the structural dynamics of the system.
- Directivity study. Using a microphone array (in an anechoic room), a directivity study of the radiated sound could be carried out.
- Individual control of the actuators. For the results presented in this report, all the actuators were connected to the same input signal, and the feedback control and feedforward filter were applied to the single signal. Individual control of the actuators will involve a more complex control algorithm, but it will probably increase the efficiency.
- Use decentralized control. Closely connected to the last point. Decentralized control of the actuators could reduce the computational complexity.
- Take a closer look into the feedback control loop. The use of an active compensator, like discussed in [32, chap. 5] could increase the stability for higher gain values.
- Design a better feedforward filter. As said before, the loudspeaker does not show second order behaviour in the low frequencies. A better designed (higher order) filter could accomplish the desired correction.
- Use modal patterns for sound generation. This would make the system a combination between a conventional driver and a distributed mode loudspeaker. This would involve the individual control of the actuators.
- Produce stereo sound and beam sound. Driving the actuators in such a way that stereo sound is produced (or beamforming) is other of the applications of the individual control of the actuators.
- Implement everything in an FPGA. This would make the prototype portable, and could perform the filtering in real time, for demonstrations.

For a new, better device, some aspects could be taken into account

- Dimensions of the plate. For this work, the size was constrained by the laser cutting machine at the University of Twente, where the perforated plate is fabricated. A more extensive research is expected to provide external possibilities in industries in the neighbourhood to make a bigger or cheaper design.

- Position springs. The solution implemented for this prototype is far from elegant. In future devices, the springs could be implemented inside the cavity, of even in the coil.
- Compliance of the air. For this prototype, the air cavity plays a major role in the frequency response. If the application is in large surfaces (for instance room walls), the volume of air is much larger. A system could be designed to simulate this unconstrained volume (for instance a (system of) hose(s) going from the enclosure to a point where the radiated sound does not interfere with the measurements.
- Design the amplifier and speaker as an integrated system, for improving the performance (impedance match, etc).

Chapter 7

Acknowledgements

First and foremost, I want to express my sincere gratitude to my daily supervisor, Arthur Berkhoff, who first introduced me to this project, and whose support and academic knowledge helped me through the whole process of this project. A special word of thanks also goes to Erwin Kuipers who was a crucial link in helping me to understand mechanical aspects of structures I was not familiar with. I am also deeply indebted with Henny Kuipers, who plaid an essential role in the building and installation of the whole device. Without his work and his experience, this thesis would not exist. The assistance of Gert Jan Laanstra with the digital aspects of the measurements and with the Xenomai platform was also crucial. Without him, I would probably still be lost in the world of big endians, LSB's and cyclic buffers. I am also truly grateful with Bert Wolbert, whose help and explanations in conducting the structural experiments were of incalculable value. Thanks also to Mark Herink and Sjoerd van Ophem, who previously worked on this project, and who I was welcome to consult at any moment. Last but not least, I want to thank the Structural Dynamics and Acoustics group for allowing me to use their knowledge and facilities and the whole Signals and Systems group for help and support in the daily work, and for providing me with an enjoyable work environment.

Bibliography

[1] http://www.glas-platz.de/.

[2] http://www.polypower.com/.

[3] http://www.sonance.com/.

[4] http://www.soundadvance.com/.

[5] Nxt technology review, 2002.

[6] Press release: New flat flexible speakers might even help you catch planes & trains, March 2009. Last retrieved: 18-07-2011.

[7] Press release: Ultra-flat loudspeakers with powerful sound reproduction, September 2009. Last retrieved: 18-07-2011.

[8] 14th International Convention on Experimental Mechanics (ICEM), Poitiers, France. *Identification of honeycomb sandwich properties by high-resolution modal analysis*, July 2010.

[9] 4th international workshop on wearable and implantable body sensor networks. *EMFi in wearable audio applications*, 2007.

[10] F. O. Ailish O'Halloran and P. McHugh. A review on dielectric elastomer actuators, technology, applications, and challenges. *Journal of applied physics*, 104:071101(1)–071101(10), 2008.

[11] D. H. A.P. Medley, D.R. Billson and L. Davis. Properties of an electrostatic transducer. *Journal of the Acoustical Society of America*, 120(5):2658–2667, November 2006.

[12] H. Azima. Flat speaker delivers volumes of sound, August 2004. Last retrieved: 25-07-2011.

[13] L. L. Beranek. *Acoustics*. Acoustical Society of America, New York, 1996.

[14] A. P. Berkhoff. A flat loudspeaker using a semi-porous honeycomb structure.

[15] A. P. Berkhoff. Impedance analysis of subwoofer systems. *Journal of the Audio Engineering Society*, 42(1/2):4–14, 1994.

[16] A. P. Berkhoff. Sound generator, 2008.

[17] A. P. Berkhoff. Lecture notes signal processing in acoustics and audio, November 2010.

[18] A. P. Berkhoff. Signal processing in acoustics and audio, lecture 8: Loudspeakers, December 2010.

[19] D. T. Blackstock. *Fundamentals of physical acoustics*. John Wiley & Sons, INC., 2000.

[20] P. Breedveld. *Integrated modeling of physical systems*. University of Twente, 2006.

[21] J. D. B. Keele. Low-frequency loudspeaker assessment by nearfield sound-pressure measurement. *Journal of the Audio Engineering Society*, 22(3):154–162, 1974.

[22] S. Elliott. *Adaptive structures*. John Wiley & Sons, INC., 2007.

[23] M. Herink. Flat subwoofer design - B.Sc. assignment. Technical report, University of Twente, 2011.

[24] A. A. Janszen. An electrostatic loudspeaker development. *Journal of the Audio Engineering Society*, 3:87–90, 1955.

[25] S. E. A. D. M. J. Brennan, J. García-Bonito and R. Pinnington. Experimental investigation of different actuator technologies for active vibration control. Technical report, Institute of Sound and Vibration Research, University of Southampton, 1998.

[26] D. Y. Maa. Microperforated panel wideband absorber. *Noise control engineering journal*, pages 77–84, 1987.

[27] N. Mackenzie. Distributed mode loudspeakers. In *Innovation in Acoustics and Vibration*, pages 400–405. Australian Acoustical Society, November 2002.

[28] L. Meirovitch. *Fundamentals of Vibration*. McGraw-Hill, 2001.

[29] J. L. Mika Paajanen and K. Kirjavainen. Electromechanicalfilm (emfi) - a new multipurpose electret material. *Sensors and Actuators*, 84:95–102, 2000.

[30] R. Normandin. Extended low-frequency performance of existing loudspeaker systems. *Journal of the Audio Engineering Society*, 32(1/2):18–22, 1984.

[31] H. F. Olson. *Acoustical engineering*. D. van Nostrand Company, Inc., 1957.

[32] A. Preumont. *Vibration control of active structures - An introduction*. Kluwer academic, 1997.

[33] A. Putra. Sound radiation from a perforated plate. Technical report, Institute of Sound and Vibration Research, 2007.

[34] A. Putra and D. Thomson. Sound radiation from perforated plates. *Journal of Sound and Vibration*, 329:4227–4250, 2010.

[35] J. E. Richard Heydt, Ron Pelrine and R. Kornbluh. Acoustical performance of an electrostrictive polymer film loudspeaker. *Journal of the Acoustical Society of America*, 107(2):833–839, February 2000.

[36] J. E. Richard Heydt, Roy Kornbluh and R. Pelrine. Design and performance of an electrostrictive-polymer-film acoustic actuator. *Journal of Sound and Vibration*, 215:297–311, 1998.

[37] G. Shi and P. Tong. The derivation of equivalent constitutive equations of honeycomb structures by a two scale method. *Computational mechanics*, 15(5):395–407, 1995.

[38] R. H. Small. Direct-radiator loudspeaker system analysis. *IEEE transactions on audio and electroacoustics*, 19(4):269–281, 1971.

[39] SPIE Smart Structures and Materials Symposium. *Electro-active polymers: current capabilities and challenges*, volume 4695, 2002.

[40] SPIE Vol. 6168, 61681M. *Sound radiation properties of dielectric elastomer electroactive polymer loudspeakers*, 2006.

[41] K. E. Ståhl. Synthesis of loudspeaker mechanical parameters by electrical means: A new method for controlling low-frequency loudspeaker behavior. *Journal of the Audio Engineering Society*, 29(9):587–596, 1981.

[42] H. Tijdeman. Lecture notes advanced dynamics - structural vibrations. University of Twente - Department of mechanical engineering.

[43] S. van Ophem. Modelling of a flat loudspeaker. Technical report, TNO Technical Sciences, 2011.

[44] D. R. von Recklinghausen. Low-frequency range extension of loudspeakers. *Journal of the Audio Engineering Society*, 33(6):440–446, 1985.

[45] J. M. Wesselink. *A rapid prototyping system for broadband multichannel active noise and vibration control*. PhD thesis, University of Twente, 2009.

[46] J. X.-d. Xia Li-juan and W. Yang-bao. The equivalent analysis of honeycomb sandwich plates for satellite structure. *Journal of Shanghai Jiao Tong University*, 37(7):999–1001, 2003.

[47] D. Zenkert. An introduction to sandwich construction. *EMAS*, 1995.

Appendices

Appendix A

Datasheet of the coil

For Further Information Contact ....
Heason Technologies Group Ltd
Tel: +44(0)1403 755800
Fax: +44(0)1403 755810
Email: sales@heason.com
Freephone 0800 374903 www.heason.com
Heason Technologies Group

FSCM NO.	DRAWING NO.	SHEET	REV
55789	LA18-12-000A	1	B

REVISIONS

ZONE	REV	DCN NO.	DESCRIPTION	INITIALS	DATE	APPROVED
	A	010939R	INITIAL RELEASE	RLE	7/30/01	M.G.
	B	021199	UPDATE TO DUAL DIM. TITLE BLOCK	MJL	10/29/02	M.G.

WINDING CONSTANTS	UNITS	TOL	SYMBOL	WDG A
DC RESISTANCE	OHMS	±12.5%	R	2.6
VOLTAGE @ F_P	VOLTS	NOMINAL	V_P	14.9
CURRENT @ F_P	AMPERES	NOMINAL	I_P	5.71
FORCE SENSITIVITY	LB/AMP	±10%	K_F	1.75
	N/AMP	±10%		7.78
BACK EMF CONSTANT	V/FT/SEC	±10%	K_B	2.37
	V/M/SEC	±10%		7.8
INDUCTANCE	MILLI-HENRY	±30%	L	1.00

ACTUATOR PARAMETERS	UNITS	SYMBOL	VALUE
PEAK FORCE *	LB	F_P	10
	N		44.5
CONTINUOUS STALL FORCE **	LB	F_{CS}	3.4
	N		15.1
ACTUATOR CONSTANT	LB/$\sqrt{WATT}$	K_A	1.09
	N/$\sqrt{WATT}$		4.8
ELECTRICAL TIME CONSTANT	MILLI-SEC	τ_E	385
MECHANICAL TIME CONSTANT	MILLI-SEC	τ_M	1.9
POWER I^2R @ F_P	WATTS	P_P	84.9
STROKE	± INCHES		0.120
	± MM		3.0
CLEARANCE ON EACH SIDE OF COIL	IN		0.015
	MM		0.38
THERMAL RESISTANCE OF COIL	°C/WATT	Θ_{TH}	8.7
MAX. ALLOWABLE COIL TEMP.	°C	TEMP	155
WEIGHT OF COIL ASSEMBLY	OZ	WT_C	1.54
	G		43.7
WEIGHT OF FIELD ASSEMBLY	OZ	WT_F	6.2
	G		175.8

* 10 SECONDS AT 25°C AMBIENT, 155°C COIL TEMP
** 25°C AMBIENT & 155°C WINDING TEMPERATURE

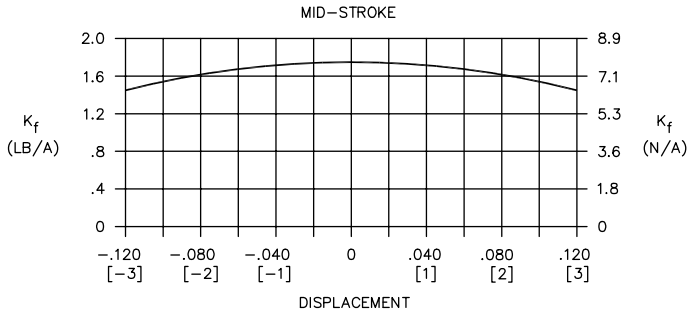

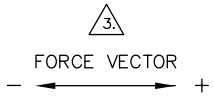

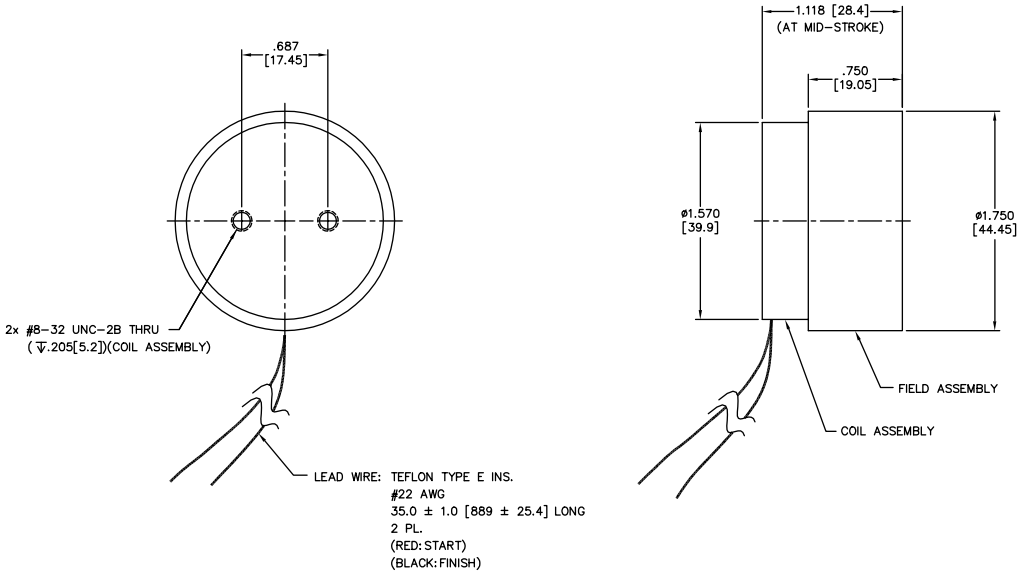

3. A POSITIVE (+) VOLTAGE APPLIED TO THE RED (START) LEAD WILL PRODUCE A FORCE ON THE COIL ASSEMBLY IN THE POSITIVE (+) DIRECTION.
2. DIMENSION IN BRACKETS ARE MILLIMETERS [MM] AND ARE FOR REFERENCE ONLY.
1. INTERPRET DIMENSIONS & TOLERANCES PER ANSI Y14.5M-1982.

NOTES: UNLESS OTHERWISE SPECIFIED

THIRD ANGLE PROJECTION

UNLESS OTHERWISE SPECIFIED:
- ALL DIMENSIONS ARE IN INCHES
- DIMENSIONS ARE AFTER FINISH

DO NOT SCALE DRAWING

TOLERANCES:
DECIMALS: .X ± 0.03, .XX ± 0.01, .XXX ± 0.005
ANGULAR: ± 0°30"

BEI KIMCO MAGNETICS DIVISION
SAN MARCOS, CA 92069

APPROVALS	DATE
DRAWN R. ELLIOTT	7/28/01
CHECKED	
APPROVED M. GODKIN	7/30/01

TITLE: LINEAR ACTUATOR

SIZE	FSCM NO.	DRAWING NO.	REV
D	55789	LA18-12-000A	B

SCALE 2/1 SHEET 1 OF 1

Appendix B

ICP amplifier

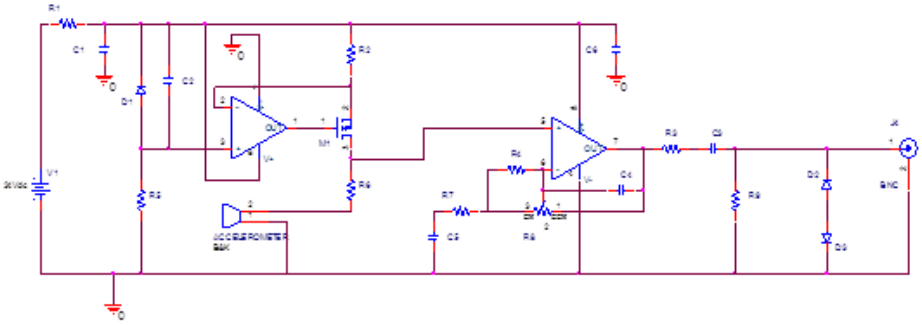

Figure B.1: *Schematics of ICP amplifier*

Appendix C

Current amplifier

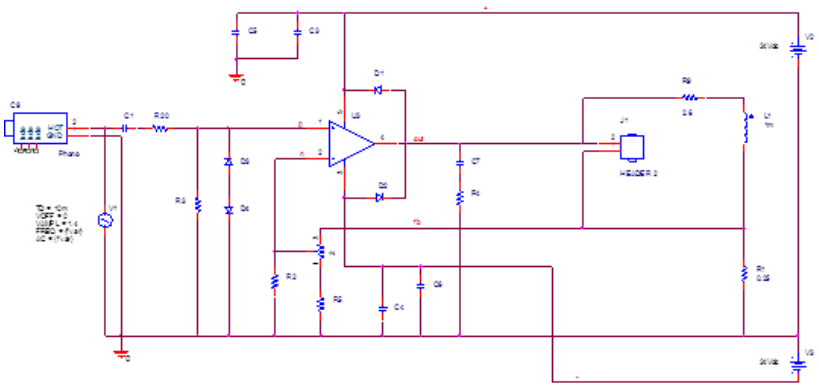

Figure C.1: *Schematics of current amplifier*

Appendix D

Datasheet of JBL P1022 10 inch woofer

P1022 10" Woofer – Technical Data

SPECIFICATIONS

Diameter:	10" (254 mm)
Sensitivity (2.83 V @ 1 m):	96 dB
Power Handling:	400 W_{RMS} 1600 W_{PEAK}
Frequency Response:	25 ~ 500 Hz
Nominal Impedance:	2 ohms (per coil)
Voice-Coil Diameter:	3.0" (76.2 mm)

Dimensions:

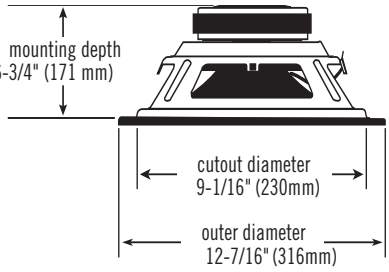

THIELE-SMALL PARAMETERS

Voice Coil Dc Resistance:	R_{EVC} (ohms) 1.00
Voice Coil Inductance @ 1kHz:	L_{EVC} (mH) 1.10
Driver Radiating Area:	S_D (in^2) 56.27
	S_D (cm^2) 363.00
Motor Force Factor:	B_L (Tm) 9.43
Compliance Volume:	V_{AS} (ft^3) 0.71
	V_{AS} (liters) 20.00
Suspension Compliance:	C_{MS} (μm/N) 106.30
Moving Mass, Air Load:	M_{MS} (grams). . . . 281.30
Moving Mass, Diaphragm:	M_{MD} (grams) . . . 277.30
Free-Air Resonance:	F_S (Hz) 29.00
Mechanical Q:	Q_{MS} 8.21
Electrical Q:	Q_{ES}. 0.58
Total Q:	Q_{TS}. 0.55
Magnetic-Gap Height:	H_{AG} (in) 0.48
	H_{AG} (mm) 12.00
Voice-Coil Height:	H_{VC} (in) 1.58
	H_{VC} (mm) 40.00
Maximum Excursion:	X_{MAX} (in) 56
	X_{MAX} (mm) 14.00

*VOICE COIL CONNECTED IN PARALLEL

SEALED ENCLUSURE VOLUME (INCLUDES DRIVER DISPLACEMENT)

P1022
(side view)

V_{BOX} = 0.75 ft^3 (21.24 liters)
(stuffed with loose-packed fiberfill)

SEALED ENCLOSURE FREQUENCY RESPONSE @ 2.83 V

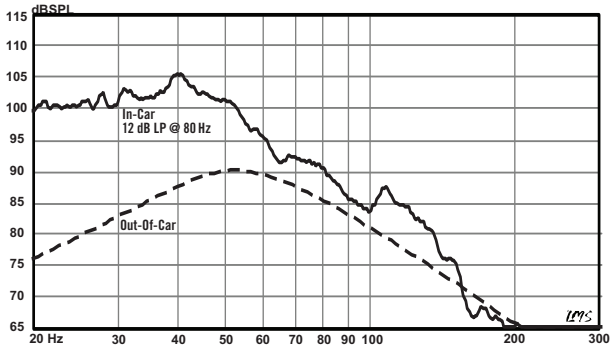

SEALED ENCLOSURE TRANSDUCER EXCURSION @ 400 W